JGR Earth Surface

RESEARCH ARTICLE
10.1029/2018JF004928

Three-Dimensional Flow Above River Bedforms: Insights From Numerical Modeling of a Natural Dune Field (Río Paraná, Argentina)

Alice Lefebvre[1]

[1]MARUM, University of Bremen, Bremen, Germany

Key Points:
- The slip face is defined as the portion of a bedform lee side with angles steeper than 15°
- Reverse flow and turbulent wake properties are linked to the characteristics of the slip face more than to bedform height
- The length of the flow separation zone and the turbulent wake are, for the tested settings, 5 and 13 times the height of the slip face

Correspondence to:
A. Lefebvre,
alefebvre@marum.de

Citation:
Lefebvre, A. (2019). Three-dimensional flow above river bedforms: Insights from numerical modeling of a natural dune field (Río Paraná, Argentina). *Journal of Geophysical Research: Earth Surface*, *124*, 2241–2264. https://doi.org/10.1029/2018JF004928

Received 24 OCT 2018
Accepted 30 JUL 2019
Accepted article online 6 AUG 2019
Published online 22 AUG 2019

Abstract Bedforms are ubiquitous features in rivers and shallow seas, as mobile sediment is transported by flowing water. The mutual interaction of hydrodynamics and bedform has been widely studied in the laboratory over two-dimensional bedforms having an angle-of-repose (30°) lee side and a relatively simple shape. However, the influence of bedform natural morphology and three-dimensionality on the flow is still poorly constrained. The present work looks at how a natural three-dimensional (3-D) bedform field influences flow properties through high-resolution numerical modeling. A 3-D numerical model is set up with Delft3D and verified against lab experiments of idealized 3-D bedforms. The model is used to simulate water velocities, turbulence, water levels, and bed shear stress above a natural bedform field from the Río Paraná (Argentina). The presence and size of the flow separation zone and turbulent wake depend on the presence and properties of the slip face (defined here as the portion of the lee side with angles >15°) and not on those of the crest. When present, the flow separation and wake lengths are, for the tested settings, respectively, around 5 and 13 times the slip face height. A slip face orientation of 25° or more compared to the flow increases cross-stream flow and suppresses flow reversal over the slip face. To understand and predict flow and bedform properties, the slip face rather than the crest position should be identified and analyzed.

Plain Language Summary In rivers and at the coast, the water flows fast and moves sand. This often forms underwater dunes, exactly like the movement of sand by wind forms desert dunes. These underwater dunes can be several meters high and are therefore a danger for navigation. They move and can be a risk for offshore structures (like wind farms). Understanding the movement of water above dunes helps to say how dunes will move. In the past, it has often been done over dunes made in the laboratory. In the work presented here, we look at how water is moving above natural dunes, which were measured in the Paraná River in Argentina. For this, we use a numerical model: A computer calculates how the water is moving above the measured dunes. We found that water movement depends on the part of the dunes which is the steepest, called the slip face. It does not depend on the highest point, the crest, as previously thought. Therefore, when studying a dune, the slip face properties should be looked at in order to say how water will move over the dune. Our work will make it easier to say how dunes and water move.

1. Introduction

Under the action of hydrodynamic forces (tidal currents, waves, and river flows), the bed can be mobilized and frequently forms rhythmic wavy features, collectively known as bedforms. Bedforms are active morphodynamic elements that both reflect and influence hydrodynamic and sediment dynamics processes at various spatiotemporal scales. The study of their presence, size, movement, and interaction with the flow is directly relevant for a wide range of applications such as the dynamics of mine burial, the impact of marine aggregate extraction, the safety of offshore structures, the protection of cables, and the control of navigational depth.

Traditionally, the effect that bedforms have on the flow has been investigated in laboratory flumes over two-dimensional (2-D) bedforms having an angle-of-repose (30°) lee side and a relatively simple shape (triangular shape or a sinusoidal stoss side and a straight lee side). Over such bedforms, the flow field can be categorized in different regions with specific characteristics that have fundamentally distinct effect on flow and sediment transport (Figure 1a; see reviews by Best, 2005, and Venditti, 2013): (1) a flow separation zone (FSZ) over the bedform lee side in which reverse flow is observed; (2) a shear layer and turbulent wake

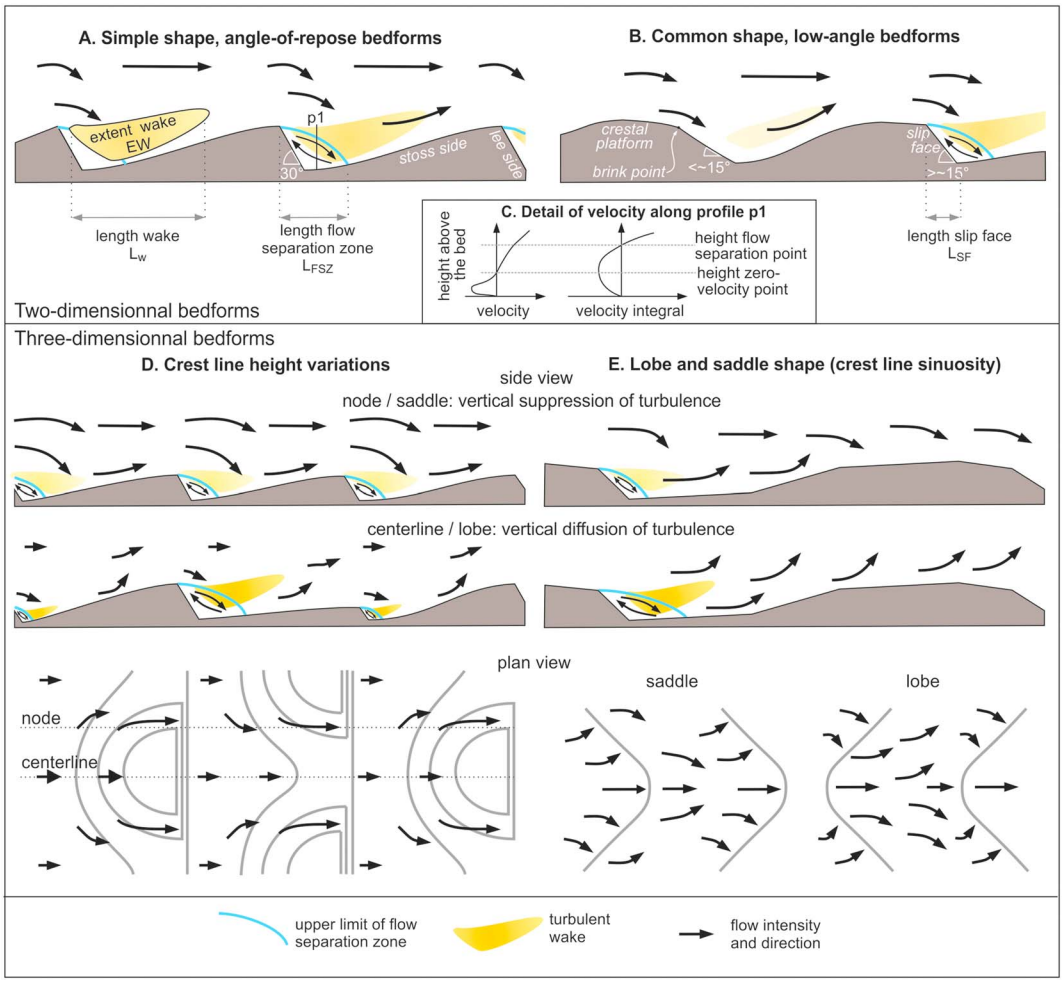

Figure 1. Summary over mean flow and turbulence above (A) 2-D simple shape, angle-of-repose bedforms, (B) 2-D common shape, low-angle bedforms, (D) 3-D bedforms with crest line height variations and (E) 3-D bedforms with lobe and saddle shapes; details of velocity along profile p1 is shown in (C) to highlight how the height of the flow separation point is found.

region, originating at the crest, extending, and expanding downstream; (3) an internal boundary layer that grows beneath the wake, from the reattachment point toward the crest; and (4) an outer, overlying region. The FSZ and associated turbulence production at the shear layer and dissipation in the wake are largely responsible for the so-called form roughness, which constitutes an important part of the shear stress in environments where bedforms are present (Kostaschuk & Villard, 1996; Lefebvre & Winter, 2016; Smith & McLean, 1977) and thus a major factor in the calculation and prediction of hydrodynamics and sediment transport.

Natural bedforms often have a lee side made up of two segments, a gentle upper lee side and a steeper slip face (Figure 1b; Lefebvre et al., 2016). Over such bedforms, flow may separate at the brink point, where the slope changes from being gentle along the crestal platform to being steep at the slip face. Bedforms formed in laboratory flumes generally develop steeper slip faces than natural bedforms (Naqshband et al., 2014; Van der Mark et al., 2008), which explains why angle-of-repose bedforms have been intensively studied in the laboratory. However, it is now recognized that many large rivers and coastal environments are characterized by bedforms with lee side or slip face slopes lower than the angle-of-repose, the so-called low-angle bedforms (Best, 2005). Over such bedforms, flow does not separate, and no permanent flow separation is observed (Best & Kostaschuk, 2002; Kostaschuk & Villard, 1996). No distinct wake is found, only a region of slightly elevated turbulence (Lefebvre et al., 2016). A wide range of slip face angles is encountered over field

bedforms, and whether flow is separating is often difficult to determine. Based on numerical modeling of flow over triangular bedforms, Lefebvre and Winter (2016) suggested that flow separation is permanent for slip face angles steeper than 11–18°, depending on bedform relative height (bedform height compared to water depth). From laboratory measurements of flow over fixed bedforms, Kwoll et al. (2016) concluded that a permanent flow separation exists only over slip face angles of 30°, and a small intermittent FSZ is present over bedforms with slip faces of 10° and 20°. These recent results based on systematic studies confirmed previous results indicating that flow separation is permanent for lee side slopes larger than 10–20° (Best & Kostaschuk, 2002; Kostaschuk & Villard, 1996; Paarlberg et al., 2007).

Bedforms are particularly abundant in rivers and in shallow tidal environments, where they develop into vast fields with a complex morphology. Fields of large bedforms are inherently three-dimensional, which is seen as crest line discontinuity (bifurcations and terminations), crest line sinuosity, crest line height variations, scour pits in the trough and spurs. Three-dimensionality may be created by various processes, for example, high flow velocity (Southard & Boguchwal, 1990), across-variations in sediment size (Ernstsen et al., 2005), presence of cohesive forces in the sediment (Baas et al., 2016; Malarkey et al., 2015), differential bedform migration rates (Fraccascia et al., 2016), or simply enough time to evolve to be three-dimensional (Baas, 1994; Venditti et al., 2005). Actually, Rubin (2012) argued that bedforms are characteristically three-dimensional and only special conditions, which induce along-crest coupling processes, may be strong enough to overcome the tendency to three-dimensionality and result in 2-D bedform fields.

Bedform three-dimensionality has been recognized by the early work of Allen (1968), who showed that it adds considerable complexity by modifying flow patterns. However, since then, only some aspects of three-dimensionality have been systematically studied: the influence of crest lines sinuosity and height variations (Maddux et al., 2003; Omidyeganeh & Piomelli, 2013; Venditti et al., 2005); and this only over geometric regular pattern and at laboratory scale, with the notable exception of the field study of Parsons et al. (2005).

Similarities of flow above bedforms with crest lines with sinuosity and height variations can be recognized (Figures 1d and 1e). Maddux et al. (2003) conducted extensive laboratory-based measurements above fixed angle-of-repose "quasi 3-D" bedforms having straight crest lines but heights that varied in the cross-stream direction (Figure 1d). Over these, the centerline was defined as the line in the center of the domain where bedform height varies the most, and the node, halfway between the centerline and the side, along which the bedform height does not vary. Venditti (2007) measured flow profiles over fixed 3-D angle-of-repose bedforms having lobe and saddle shapes. Lobes have reverse closure of their crest lines and saddle forward closure (Figure 1e). Over the node or a saddle shape, stream-wise flow is accelerated and cross-wise flow relatively high, with a strong downward-directed vertical flow. A vertical suppression of turbulence is induced with a reduced FSZ and suppressed wake. Over the centerline or lobe shape, cross-stream flow is limited, and vertical flow is positive. Flow separation and wake are strong and diffused upward. Venditti (2007) also showed the importance of upstream bed configuration as he observed no flow separation and turbulent wake over irregularly placed bedforms.

Numerical models have been used to simulate the interaction of bedforms and hydrodynamics (El Kheiashy et al., 2010; Khosronejad & Sotiropoulos, 2014; Lefebvre, Paarlberg, & Winter, 2014; Omidyeganeh & Piomelli, 2013; Stoesser et al., 2008). They compensate for limitations in field and flume measurements as they allow simulations of high-resolution near-bed flow fields, provide estimate of turbulence, and can be used with a variety of boundary conditions. Two main types of modeling approaches are available: large-eddy simulation (LES) and Reynolds-averaged Navier-Stokes. Reynolds-averaged Navier-Stokes models use a turbulence closure model to parameterize the contribution of the turbulent motions (eddies) and simulate the time-averaged flow. Therefore, flow intermittency and coherent flow structure cannot be studied with such models. On the other hand, they are computationally inexpensive. Because the computational time does not depend on Reynolds number, simulations can be run at field scales even at high-resolution (thus avoiding scaling issues). LES models compute exactly the contribution of large turbulence structures and model only the effect of the smallest scales of turbulence (Stoesser, 2014). The great advantage of LES modeling of flow over bedforms is the possibility to investigate in details coherent flow structures such as boils (Omidyeganeh & Piomelli, 2013; Stoesser et al., 2008) and of time-dependent flow separation, that is, investigate in details intermittent flow reversal. However, LES simulations are expensive in terms of

computational time, even when carried out at laboratory scale in order to keep low Reynolds numbers (Stoesser, 2014), and until recently, they were only used at laboratory scale. The review from Sotiropoulos and Khosronejad (2016) provides a detailed account of the recent advancement in the field of multiscale bedform modeling using LES coupled with morphodynamics. It highlights in particular the role of turbulence and bed shear stress fluctuations in the initiation and development of bedforms and the formation of coherent structures (Khosronejad & Sotiropoulos, 2014) and the formation of barchan dunes under finite sand supply (Khosronejad & Sotiropoulos, 2017). The evolution and migration of large dunes at river scale is now also possible using an unsteady Reynolds-averaged model coupled with a technique for decoupling the time steps of the flow from that of the sediment transport (Khosronejad et al., 2015). These recent advances in LES modeling show that LES can be used to simulate dune formation and evolution at a variety of scales in a realistic way and help elucidating the prominent role of small-scale turbulence in bedform initiation and migration.

Numerical simulation results have confirmed and detailed results from laboratory studies. Omidyeganeh and Piomelli (2013) performed high-resolution LES modeling of flow over angle-of-repose flume-scale bedforms having saddles and lobes in a setting similar to Venditti (2007). Nine cases were simulated with a bedform having more or less pronounced lobes and saddles. In most cases with in-phase crest lines, flow patterns were similar to those recognized by Venditti (2007). In the case where the bedform length was shorter than the water depth, the flow resembled that in 2-D bedforms, with a notable absence of secondary flow. When saddles and lobes were staggered, faster flow was found in the node rather than at the saddle and lobe positions, as already observed by Maddux et al. (2003). The average value of the reattachment length was lower for 3-D cases than the corresponding 2-D case due to the effect of the stream-wise vortices.

The patterns of mean and turbulent flow over angle-of-repose 3-D bedforms with regular geometrical crest lines and subjected to unidirectional flow are therefore well described (Figure 1). However, very little is still known about natural morphologies, where saddles and lobes are unlikely to be aligned or staggered. Certainly, the bed configuration of Venditti (2007) with irregular crest lines showed that the position of upstream crest lines and morphology have a strong influence on flow. One notable study focused on investigating the flow structure over full size 3-D bedforms: Parsons et al. (2005) measured bathymetry and flow velocity over a transect crossing large asymmetric bedforms in the Río Paraná, Argentina. They found that FSZs were smaller over both lobe- and saddle-shaped bedforms (having lee side angles of around 14°) than over 2-D bedforms. Their results concurred with Venditti (2007) lab results with respect to the lobe pattern but contradicted the findings over the saddle pattern. They also conclude that bedform three-dimensionality is connected to the morphology of the upstream bedform, with changes in crest line curvature and crest line discontinuities significantly influencing the downstream bedform. The results of Parsons et al. (2005) contributed to the understanding of flow over natural bedform fields with lee side angles lower than the angle of repose. However, they were limited in their analysis because the flow was measured over only one transect, and therefore, they were not able to correctly resolve lateral flows. Furthermore, they could not collect flow velocity measurements close to the bed or calculate turbulence above the bedforms due to instrumental limitations. As a result, it was not clear whether flow separation above the saddle/lobe shape was not detected because flow separation was affected by the 3-D morphology or because of the instrument resolution (Parsons et al., 2005).

Although bedform three-dimensionality and its influence on the flow are widely recognized, little is still known about the interaction of natural bedform three-dimensionality and the flow field. This is largely due to the difficulty in recording precise concomitant measurements of 3-D flow and turbulence in the field, as observed by Parsons et al. (2005). Flume-based studies can provide detailed high-frequency measurements of velocity and turbulence over 3-D bedforms. However, reproducing complex natural bed morphology and flow properties at adequate spatial and time scales is problematical. Despite their limitations, numerical models provide a complementary approach to laboratory and field measurements to better understand flow fields over complex bedform fields.

The present work aims to understand how a natural three-dimensional bedform field influences flow velocities and turbulence through high-resolution numerical modeling. Ultimately, the purpose is to determine significant relations between flow properties and bedform morphology in order to estimate the presence and size of flow separation and turbulent wake based on bathymetric maps. The Delft3D numerical modeling

system is used to simulate 3-D flow above natural bedforms. The model is first verified against Maddux et al. (2003) lab data before being used to model 3-D flow velocities and turbulence above a bedform field from the Río Paraná (Argentina) previously described by Parsons et al. (2005).

2. Modeling System and Data Analysis

2.1. Delft3D Modeling System

Delft3D is an open-source integrated modeling system developed to simulate flow and transport for river, estuarine, and coastal areas. In the Delft3D-FLOW module, the 3D nonlinear shallow water equations derived from the three-dimensional Reynolds-averaged Navier-Stokes equations for incompressible free surface flow are solved by using a turbulence closure model (Deltares, 2014). In order to capture nonhydrostatic flow phenomena such as flow recirculation on the lee of bedforms, the nonhydrostatic pressure is computed by using a semi-implicit finite difference model for nonhydrostatic flows (Casulli, 1999): For every time step, provisional velocities and water levels are calculated by neglecting the contribution of the nonhydrostatic pressure. In a second step, the nonhydrostatic pressure terms are included to correct the provisional values, and the final velocities and water levels are computed. Details of the correction technique can be found in Deltares (2014).

The nonhydrostatic Delft3D modeling system has already been successfully used to set up a 2-D vertical numerical model to simulate horizontal and vertical velocities, turbulent kinetic energy (TKE), and water levels above fixed bedforms. The model has been calibrated and validated against the laboratory flume experiments of McLean et al. (1999) and proved to correctly reproduce horizontal and vertical velocities (including flow separation), turbulence, and shear stress over idealized, angle-of-repose bedforms under unidirectional flow conditions (Lefebvre, Paarlberg, & Winter, 2014). Further confirmed against field data, the model also showed to correctly simulate velocities, TKE, and water levels in a tidal environment over natural bedforms (Lefebvre, Paarlberg, Ernstsen, et al., 2014). It has also been used to carry out systematic experiments to constrain the influence of lee side angle on bedform roughness (Lefebvre & Winter, 2016) and to characterize the effect of natural bedform morphology on flow (Lefebvre et al., 2016). Details of the 2-D model setup, calibration, and validation, including specifics on the turbulence closure scheme and sensitivity to grid size and roughness length, can be found in Lefebvre, Paarlberg, Ernstsen, et al. (2014), Lefebvre, Paarlberg, & Winter (2014).

2.2. Model Setup

The model is now set up to simulate three-dimensional flows over bedform fields by extending the model domain into the cross-stream direction. Since the model calibration in 2-D, the FLOW module of Delft3D has been updated (Deltares, 2014). Delft3D-FLOW now offers the functionality to remap the near-bottom layers in order to reduce the inaccuracies and discontinuities in bottom shear stress and velocity profiles associated with the z-layer model (Platzek et al., 2014).

All simulations are performed on a 3-D Cartesian model grid discretizing a fixed bed, that is, no sediment transport is modeled. The following conditions are prescribed constant in time at the lateral open boundaries of the model domain: a logarithmic velocity profile at the upstream boundary and a water surface elevation of 0 m at the downstream boundary. The bed roughness is defined as a uniform roughness length z_0. The time step is varied depending on grid settings to follow a Courant Friedrich Lewy criterion $\mathrm{CFL} = \Delta t \sqrt{(gh)} / \{\Delta x, \Delta y\} < 10$ where t is the time step, g is the acceleration due to gravity, h is the water depth, and x and y are characteristic sizes of the horizontal grid. Since the z model is used, the following condition also applies $\Delta t \leq \min(\Delta x, \Delta y) / \max(|u|, |v|)$ where $|u|$ and $|v|$ are characteristic values of horizontal velocities (Deltares, 2014). In order to use the nonhydrostatic pressure correction technique, the model is set up with the z-grid coordinate system instead of the commonly used boundary fitted σ coordinate system (Deltares, 2014). The Cartesian coordinates system (z model) is made of fixed horizontal coordinate lines, separating the layers, and is fitted at the bottom boundary by a staircase bed. The layer thickness is defined as the distance between two consecutive z-grid surfaces. Vertical resolution for each layer depends on layer size, which can vary through the water column (non-equidistant layers).

2.3. Data Analysis

In all simulations, the x direction is defined as being stream-wise, the y direction cross-wise (positive cross-stream velocity going anticlockwise from stream-wise), and z direction vertical, with positive velocities going upward. The horizontal zero is set at the beginning of the domain or at the position of the lab measurements for the verification simulations. The vertical zero is set at the lowest position of the bed.

The analyzed model outputs are the water level, the 3-D velocities, the TKE, and the bed shear stress. The presence of flow separation is detected as negative stream-wise flow. For each point at the bed where a negative stream-wise velocity is found, the height of the FSZ is calculated as the distance above the bed at which the net discharge per unit width is zero (Figure 1c). In other words, the height of the FSZ is situated where the integral of the negative velocity between the bed and the zero-velocity point is compensated by the integral of the positive velocity between the zero-velocity point and the height of the flow separation (Lefebvre, Paarlberg, & Winter, 2014; Paarlberg et al., 2007).

3. Sensitivity Analysis and 3-D Model Verification

A sensitivity analysis is carried out on a bed made of 14 bedforms with straight crest with varying height, as studied by Maddux et al. (2003) in the lab (Figure 2) but scaled 50 times larger, that is, mean wavelength L_b = 40 m and mean height H_b = 2 m (Table 1), in order to reduce simulation times by setting a larger time step (which depends on the horizontal grid following the CFL and the z-model recommendation). Specifically, the parameters tested were turbulence closure model, boundary conditions (discharge or velocity, including logarithmic or uniform velocity profile and reflection parameter alpha), smoothing time, advection scheme for momentum, background horizontal viscosity, time step, remapping of bottom layers, simulation length, horizontal grid, number and distribution of vertical layers, roughness length, and additional parameters from the nonhydrostatic settings (full or weak, maximum number of iterations, and stop criterion CG (conjugate gradient) method; see Deltares, 2014, for details). Only the most relevant results are presented and discussed here.

The tests of model settings revealed that only the k-ε turbulence closure model (Deltares, 2014) gives satisfactory results. The other turbulence models give patterns of flow above the bedforms that do not represent what Maddux et al. (2003) measured. A calibration parameter of Delft3D-FLOW is the background horizontal viscosity, which depends on flow velocity and grid size (Deltares, 2014). It was determined that a value of 0.001 m^2/s or lower gives good results at field scale. At lab scale, a value of 0.000001 m^2/s or lower should be used. As already identified in the 2-D model (Lefebvre, Paarlberg, & Winter, 2014), the results are strongly influenced by the horizontal and vertical resolutions, which need to be fine enough to resolve flow separation and recirculation over the bedform lee. The layer size should be small near the bed in order to successfully capture processes relevant to 3-D flow above bedforms and may be gradually increased toward the water surface. The model is found to be only marginally sensitive to the time step as long at the CFL and z-model recommendation are followed. For example, the time step for a model with $x = y$ = 0.03 m, water depth h = 8 m, and $\max(|u|,|v|)$ = 1 m/s would be recommended to be equal or inferior to 0.3 s. In this case putting dt = 0.6 s results in unstable simulation. Simulations with dt = 0.3 s or dt = 0.15 s both work well, with results having a velocity difference of less than 1% or 0.0005 m/s. Roughness length had a strong influence on flow separation and turbulent wake length, with in general, a decrease in flow separation and wake size with increasing roughness, as already observed with a similar model in 2-D (Lefebvre, Paarlberg, & Winter, 2014, see in particular Figures 8 and 9).

The model is then verified against the data from Maddux et al. (2003), which consists of laboratory-based velocity and water surface measurements above 3-D bedforms. The measurements were made in the 22-m-long recirculating flume in the Ocean Engineering Lab at the University of California, Santa Barbara, over 14 fixed artificial bedforms (mean wavelength = 0.8 m, mean height at the crest = 0.04 m, a half-cosine shaped stoss side, and a straight angle-of-repose lee side) roughened with coarse sand. The three-dimensionality of the bedforms was established as a full cosine wave in the cross-stream direction, superimposed on the profile of the 2-D bedforms (Figure 2). Successive crest lines were staggered, so that a bedform with a high middle and low sides was followed immediately by a bedform with a low middle and high sides. Detailed measurements of velocity and free surface topography were performed over the eleventh and twelfth bedforms, from the bed to the free surface and from the centerline of the flume to

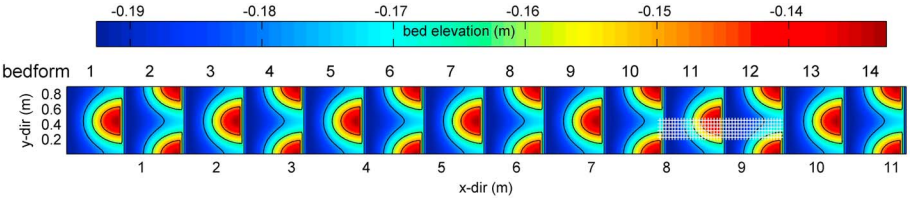

Figure 2. Bed configuration of the Run T2 (Maddux et al., 2003) which is used to verify the 3-D numerical model. The bed contains 14 fixed bedforms (mean wavelength = 0.8 m, mean height at the crest = 0.04 m, a half-cosine-shaped stoss side, and a straight angle-of-repose lee side) with a full cosine wave in the cross-stream direction to produce three dimensionality. The crosses over the eleventh and twelfth bedforms show where measurements were taken.

the halfway point between the centerline and the wall (Figure 2). Vertical profiles were spaced every 0.04 m in the x direction and every 0.045 m in the y direction with an approximately logarithmic spacing relative to the local bed elevation, starting from a few millimeters off the bed, for a total of between 20 and 30 data points, depending on the local flow depth. The mean water depth was 0.173 m and the averaged velocity 0.357 m/s (Table 1). To verify the numerical model, the whole bed configuration tested in the laboratory (Figure 2) is set as the model bed, with a horizontal resolution of 0.01 m and 37 non-equidistant layers (over 3.8 million points modeled). The average velocity is used as entrance boundary condition until the model reaches stability. Two values of roughness length are tested, $z_0 = 0.0001$ m and $z_0 = 0.0002$ m, to estimate the influence of roughness on the results. These values are selected to resemble the roughness in the laboratory experiments where the bedforms were roughened with coarse sand of 1 mm in diameter sprinkled on wet paint. Assuming $z_0 = d_{50}/12$ where d_{50} is the median grain diameter (Soulsby, 1997), this would suggest that z_0 in the experiment was around 0.00008 m.

For a precise assessment of how well the model simulates the laboratory data, the mean absolute and relative differences (MAD and MRD) between the modeled and measured quantities are calculated for each measurement as $\boldsymbol{MAD}=\overline{|lab_i - sim_i|}$ and $\boldsymbol{MRD}=\overline{(lab_i - sim_i)/lab_i}$ where lab_i represents a laboratory measurement and sim_i the corresponding simulated parameter. MAD and MRD are calculated for the depth-averaged quantities, along the six profiles measured by Maddux et al. (2003) and for all the available measurements. Table 2 shows MAD and MRD between modeled and measured data for the largest roughness length tested, $z_0 = 0.0002$ m, as it gives the smallest overall difference between the measured and modeled data. Figures 3 and 4 show the comparison of this simulation with the laboratory measurements for the depth-averaged quantities and for profiles at the centerline and node. Table 2 summarizes the MAD and MRD between the laboratory measurements and model simulations. The measured and modeled water levels show similar patterns, with high water level over the middle stoss side and low water level over the crest and lee side (Figures 3a–3c). As observed by Maddux et al. (2003), stream-wise velocities are lowest over the centerline (where the bedform heights are varying the most) and largest over the node (where the flow experience

Table 1
Summary of Model Settings

Parameter	Sensitivity analysis	Model verification	Paraná dune field
Bedform shape	Straight crest line with height variations	Straight crest line with height variations	Natural bedform field
Bedform size	mean length = 40 m; mean height = 2 m	mean length = 0.8 m; mean height = 0.04 m	Mean length = 57 m; mean height = 1.25 m
Water depth (m)	8	0.17	6.4
Input velocity (m/s)	1	0.32	Range tested: 0.85 to 1.15
Horizontal resolution (m)	Range tested: 0.3–1	0.01	0.5
Number of layers (corresponding vertical resolution)	Range tested: 30–60 (0.2–0.06 to 0.6–0.4 m)	37 (0.003 to 0.015 m)	40 (0.15 to 0.47 m)
Background horizontal viscosity (m^2/s)	Range tested: 10^{-7}–1	10^{-6}	10^{-3}
Time step (min)	Range tested: 0.001–0.01	0.00008	0.0025
Roughness length (m)	Range tested: 0.0001–0.005	0.0001	Range tested: 0.000001–0.02

Table 2
Mean Relative Difference (MRD) and Mean Absolute Difference (MAD) of Stream-Wise (U), Cross-Stream (V), and Vertical (W) Velocities; Turbulent Kinetic Energy (TKE); and Water Level, for the Depth-Averaged Quantities, Along the Six Profiles Measured by Maddux et al. (2003) and of All the Measured Data

	U		V		W		TKE		Water level	
Data	MAD (m/s)	MRD (%)	MAD (m/s)	MRD (%)	MAD (m/s)	MRD (%)	MAD (m^2/s^2)	MRD (%)	MAD (m)	MRD (%)
Depth-averaged	0.035	−4.3	0.0047	43.7	0.0046	57.1	0.0004	21.2		
Profile 1 (centerline)	0.061	−13.9	0.0091	27.7	0.0071	272.3	0.0126	454.6	0.00021	−8.7
Profile 2	0.049	−4.4	0.0127	48.5	0.0077	53.5	0.0125	350.3	0.00019	20.6
Profile 3	0.038	6.0	0.0119	125.4	0.0081	217.2	0.0111	10.9	0.00015	31.6
Profile 4	0.037	10.2	0.0083	117.7	0.0078	57.2	0.0090	−293.9	0.00014	2.3
Profile 5	0.065	0.8	0.0083	54.5	0.008	9.4	0.0098	−490.4	0.00013	11.3
Profile 6 (node)	0.063	23.8	—	—	0.0082	78.2	0.0102	−567.9	0.00013	5.6
Average all data	0.052	3.8	0.0091	74.7	0.0078	114.6	0.0109	−89.2	0.00016	18.1

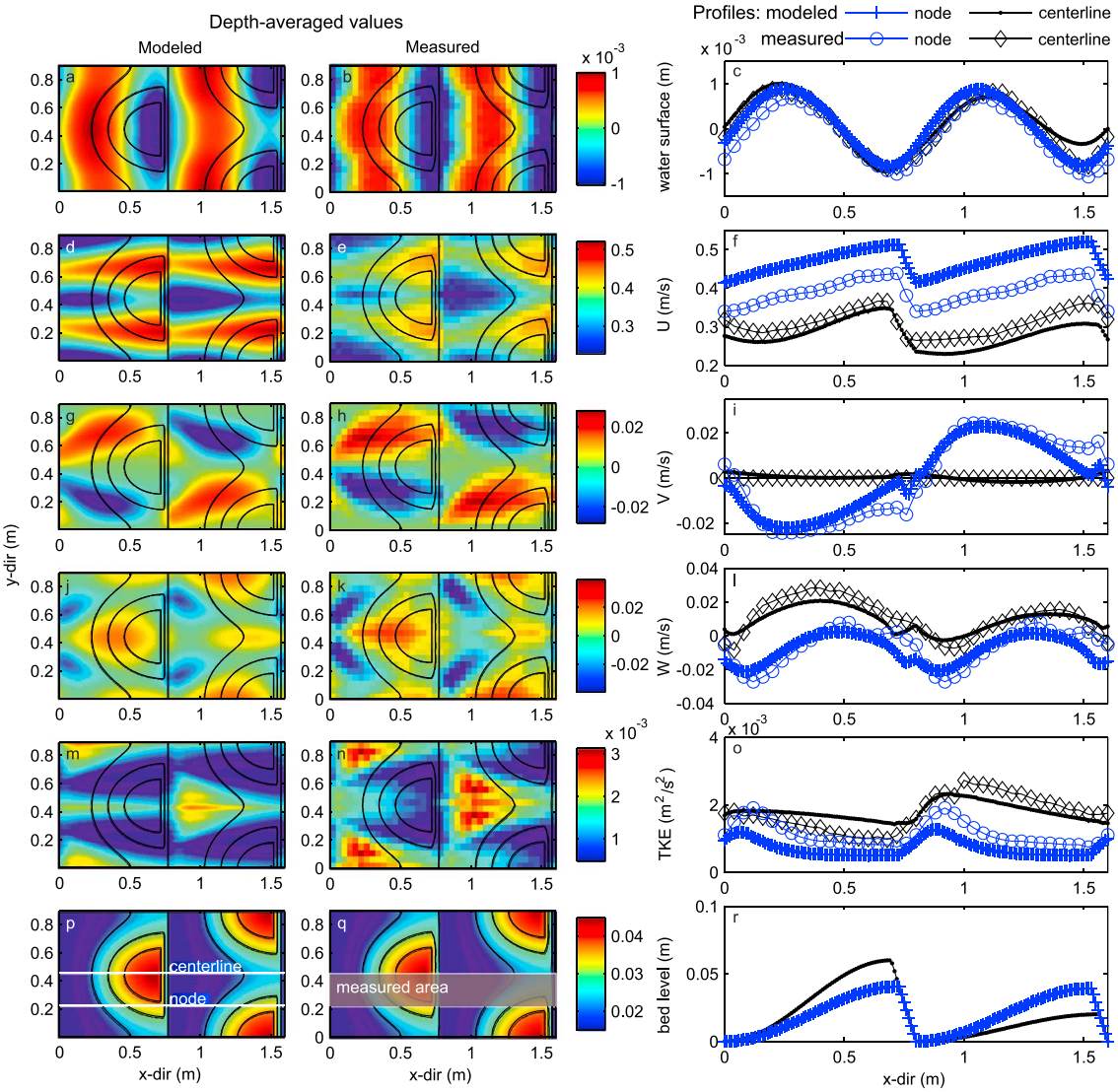

Figure 3. (a and b) Water surface, (d and e) depth-averaged stream-wise (U), (g and h) cross-stream (V), and (j and k) vertical (W) velocities; (m and n) turbulent kinetic energy (TKE); and (p and q) bed level as modeled and measured by Maddux et al. (2003) and (right) profile of the same quantities (c = water surface, f = stream-wise velocity, i = cross-stream velocity, l = vertical velocity, o = TKE and r = bed level) along the node and centerline. The depth-averaged data were intentionally not interpolated or smoothed in order to highlight the difference in available data points between the modeled and measured data.

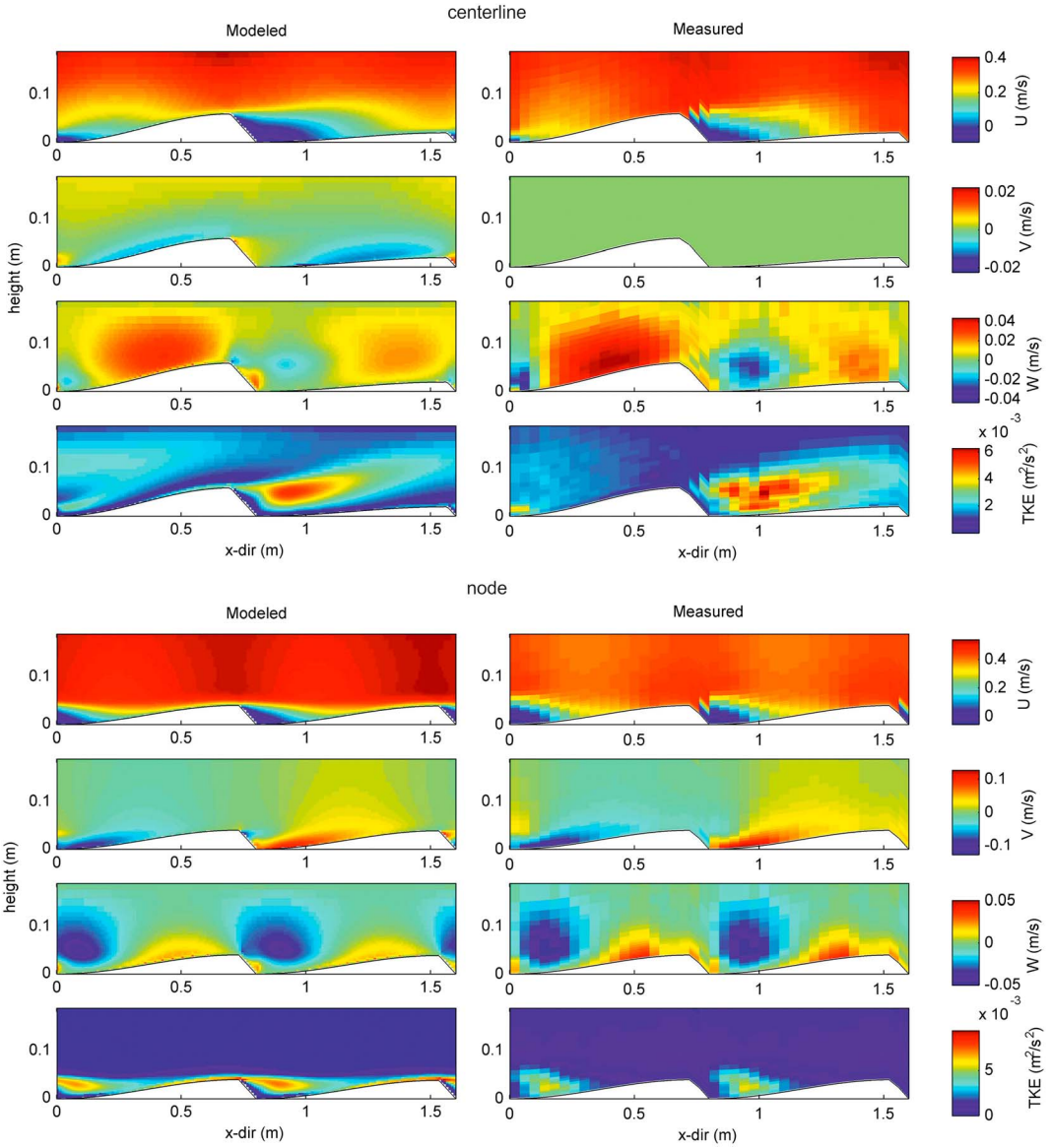

Figure 4. Profiles of stream-wise (U), cross-stream (V), and vertical (W) velocities and turbulent kinetic energy (TKE) along the centerline as modeled and measured by Maddux et al. (2003), (top) at the centerline and (bottom) at the node. The data were intentionally not interpolated or smoothed in order to highlight the difference in available data points between the modeled and measured data.

the least bed height variation; Figures 3d–3f). This can be seen for both the laboratory measurements and model results, but it is accentuated for the model simulations compared to the measurements, with the modeled stream-wise velocity over the node and centerline being on average 0.08 m/s (24%) higher and 0.03 m/s (14%) lower than the measured velocities. The difference between the measured and modeled stream-wise velocity is the highest in terms of absolute values (0.05 m/s), due to the overprediction (underprediction) of stream-wise velocity over the node (centerline), but it is the lowest MRD of the three velocities (average of 3.8% for all data; Table 2). The modeled and measured cross-stream velocities have very similar patterns and values, showing very low cross-stream velocity over the crest line and higher velocity over the node, with the bed height variations steering the flow away from the highest crest (Figures 3g–3i). The vertical velocities are also similar for the modeled and measured values, with flow generally going upward over the stoss side and downward over the lee side (Figures 3–3l). The relative difference between the measured and modeled data for the stream-wise and cross-stream velocities is in general high (between 20% and 270%). However,

the MAD is small (always less than 1 mm/s; Table 2). The TKE is high behind the highest part of the crest for both the model results and laboratory measurements (Figures 3m–3o), reflecting the position of the turbulent wake associated with flow separation (Figure 4). The relative and absolute differences between the measured and modeled TKE are relatively large (MAD = 0.01 m^2/s^2 and MRD = −89%; Table 2). The difference in TKE is likely to be related to the difference in stream-wise velocity. Above the node, stream-wise velocity near the bed is underpredicted over the stoss side, resulting in lower modeled TKE compared to laboratory measurements. On the other hand, velocity is overpredicted over the lee side, resulting in higher modeled TKE in the wake than measured. These discrepancies in stream-wise velocity and TKE between the modeled and laboratory results may be caused by inherent differences. The flume walls induce a friction, not present in the model, which may account for the overall stronger TKE in the laboratory measurements than in the model results. The model simulates Reynolds-averaged quantities, whereas the laboratory measurements are time averaged. The numerical model and laboratory measurements have different resolution and precision.

The profiles over the centerline and node (Figure 4) confirm the results observed from the depth-averaged quantities, also showing a very good agreement between the modeled and measured quantities. Over the centerline, there is vertical diffusion of turbulence, with relatively low stream-wise velocity, very low cross-stream flow (so low that Maddux et al., 2003, could not get reliable measurements), and strong upward flow over the stoss side. Flow separation over the high crest is strong, and the wake is large and extending upward. Over the node on the other hand, the strong stream-wise, low cross-stream velocities and strong downward flow over the lee side result in a vertical suppression of turbulence, and the turbulent wake is restricted in height.

The comparison of simulation results to the laboratory measurements of Maddux et al. (2003) showed that the model provides a realistic simulation of the 3-D velocity and turbulence fields over regular 3-D bedforms, with little differences between the measured and modeled quantities considering differences in setup and precision of measured velocities. The numerical model is therefore considered a suitable tool to investigate Reynolds-averaged velocities and TKE above a three-dimensional bedform field.

4. Río Paraná Bedforms

4.1. Study Site

The model is used to simulate flow over a natural bedform field collected in the Río Paraná, Argentina, by Parsons et al. (2005). Three-dimensional bathymetry of a 600-m-wide and 1.3-km-long section of the Río Paraná (Figure 5), just upstream of the confluence of the Río Paraguay, was measured in May 2004 using a multibeam echosounder and an acoustic current Doppler profiler (ADCP). At the survey area, the Río Paraná is 2.5 km wide and 5–12 m deep. At the time of survey, the discharge of the full river section was 11,000 m^3/s. Throughout the surveyed area, Parsons (2005) observed large dunes, 1.2 to 2.5 m high and 45 to 85 m long, with smaller dunes superimposed on their stoss side. Most large dunes had continuous crest lines although some discontinuities (bifurcations and terminations) were noted. Several bedform crests show pronounced curvature producing saddle and lobe shapes. Two other noticeable features were recognized at the study area (Figure 5): a bedrock that protrudes around 2 m above the bed and channel deepening toward the SSW corner of the survey area due to the presence of a large bar upstream of the study site.

Gutierrez et al. (2013) further analyzed the bathymetry collected by Parsons et al. (2005) using robust spline filters and wavelet transforms to discriminate bedform scales. Using this method, the bed morphology was separated in three units: small dunes or ripples, medium to large dunes, and bar. The ripples and small dunes were observed to get larger from the trough to the crest of the large dunes. They were relatively symmetrical with steep stoss and lee sides. The bar was found to be highly variable along the survey area and could not be represented as a plane surface. The medium-to-large bedforms were strongly asymmetrical with a gentle stoss side, a well-developed crestal platform, and a steep lee side.

Parsons et al. (2005) described the flow structure over the bedform field. The expected acceleration and deceleration patterns over the stoss and lee sides of the large bedforms were easily recognized from the ADCP data. However, flow separation was identified over only a few bedforms. This was explained by the relative gentle slope of the lee side, which suggests that the flow separation is inexistent or small, as well

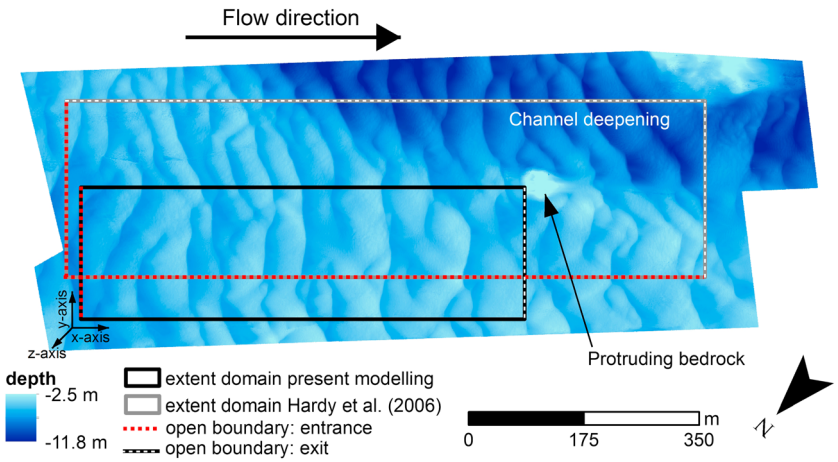

Figure 5. The Río Paraná bedform field surveyed by Parsons et al. (2005) and the extent of the domain modeled by Hardy et al. (2006) and in the present study.

as the limitations of the ADCP, which does not allow precise characterization of flow separation. Nevertheless, differences in flow direction of 15° or more between flow over the crest and lee side was detected, showing the strong topographic forcing of flow produced by the bedforms. Parsons et al. (2005) also observed that both lobe and saddle-shaped crests produced smaller regions of lee side flow separation, with higher vertical velocities, when compared with a straight-crested bedform.

A 3-D simulation of the Río Paraná bedform field has been carried out by Hardy et al. (2006) using a Reynolds-averaged k-ε RNG (Re-Normalisation Group) numerical model having a horizontal resolution of 2 m and vertical resolution of 0.25 m. The model domain comprised the channel deepening and the protruding rock (Figure 5) and had two inlets and two outlets in order to fully represent the 3-D flow, especially the cross-stream gradient. Their results showed that flow over the bedform field is considerably influenced by the meander bend and deepening of the channel which create a strong cross-stream flow, having overall more effect on the flow than the bedform field or the protruding rock (Hardy et al., 2006).

4.2. Model Setup

The present work aims to describe 3-D flow structures over natural bedforms. It does not aim to reproduce the flow condition of the whole Río Paraná bedform field, as was done by Hardy et al. (2006). The bathymetry from the Paraná dune field is here used as the basis for a natural morphology, and the flow is simulated as steady and unidirectional, with emphasis on the bedforms and not on other river features. The chosen domain size is 675 m long and 200 m wide, excluding the bedrock protrusion and deepening of the channel (Figure 5) as these are local morphological features. Hardy et al. (2006) emphasized that the dune field is situated on a river bend, creating considerable transverse flow, which is not the focus of the present work. Therefore, on the contrary to Hardy et al. (2006), the model is set up with only two open boundaries, one entrance and one exit, and two closed boundaries on the sides, in order to focus on the interaction between flow and bedforms. The model is made to resemble to some extent a field scale flume with natural bedform morphology.

The original multibeam echosounder data are rotated in order to orient the main crest lines in N-S direction, with the open boundaries at the lateral end of the domain (Figure 5). The data are gridded with a grid cell of 0.5 m, giving a domain of 400 * 1,350 cells in the horizontal. Forty non-equidistant vertical layers are set, having a size of 0.15 m from the lowest point to half a meter above the highest crest before slowly increasing to 0.45 m at the water surface. The domain is detrended to exclude any large-scale slope, and the Coriolis force is ignored. The entrance boundary (on the left) is set with a constant velocity. The depth-averaged streamwise velocity along the bedform field was around 1.0–1.3 m/s (Parsons et al., 2005). Therefore, in order to test the influence of velocity on flow properties while having realistic velocity for the prescribed bathymetry, the model is run with entrance velocities of 0.85 and 1 m/s, which results in domain-averaged velocity of 0.9 and 1.15 m/s, to represent flow conditions during which the dunes and flow are in equilibrium. A constant

water surface elevation of 0 m is prescribed at the downstream boundary. Lefebvre, Paarlberg, Ernstsen, et al. (2014) and Lefebvre, Paarlberg, and Winter (2014) showed that the chosen bed roughness length (z_0) has a prominent influence on simulated velocities and turbulence above bedforms and is therefore a crucial model setting. The median grain diameter (d_{50}) in the survey area is around 220 μm (Kostaschuk et al., 2009). The grain-related roughness length may thus be estimated by $z_0 = d_{50}/12 = 2 \times 10^{-7}$ m (Soulsby, 1997). However, secondary bedforms with maximum length of 10 m and height of 0.3 m (Parsons et al., 2005) were often observed on the stoss side of the large bedforms. These bedforms may produce a roughness $z_0 = H_b^2/L_b = 0.1$ m, where H_b is the bedform height and L_b is the bedform length (Soulsby, 1997). While grain roughness may be affecting the velocity profiles in the lower part of the velocity profiles, higher, the roughness is likely to be dominated by the influence of the secondary bedforms. As the vertical model resolution near the bed is 0.15 m, which is about the expected size of the secondary bedforms-related boundary layer, it is uncertain whether bed roughness should be set as grain roughness or as secondary bedform roughness. Therefore, roughness lengths of 10^{-6}, 10^{-4}, and 10^{-2} m are tested to determine the influence of roughness length on model results and determine which roughness gives more realistic results for this model setting.

4.3. Bedform Morphology

In order to analyze how the flow is influenced by the bedform field, the morphology of the model domain is examined in detail by doing a combination of 2-D and 3-D analysis of the bathymetry, with special interest in the slopes. The crest and trough positions of the large bedforms are determined semiautomatically. First, the 400 transects from the 0.5-m resolution bathymetry are analyzed using the Bedforms-ATM toolbox (Gutierrez et al., 2018). The results of this analysis showed that the dominant wavelength of the large bedforms is 60 m. Subsequently, a zero-crossing technique similar to the dune tracking method of Van der Mark and Blom (2007) is used on the filtered morphology of the large bedforms, targeting the dominant bedform length of 60 m (Figure 6a). Thereafter, crest and trough lines are computed by manually following the automatically detected crest and trough positions (Figure 6b). Naturally, since the final positions of the crest and trough lines are manually traced, they are sensitive to decision made by the operator. Therefore, this process is repeated several times in order to test the results sensitivity to operator decision. The results are remarkably insensitive to the manual positioning of the crest and trough lines with average values of wavelength and bedform height varying by less than 2%.

Lefebvre et al. (2016) demonstrated that the angle of the slip face, the steep portion of the lee side, controls the presence and strength of a FSZ and turbulent wake over idealized regular bedforms. The slip face is here defined as portions of the bed where the stream-wise angle is equal or larger than 15°. Its position is calculated from a 3-D analysis by detecting all portions of the whole model domain where stream-wise angles are steeper than 15°. In order to remove isolated points coming from large secondary bedforms, only portions having at least eight interconnected points are kept for analysis (86.3%).

Eighteen crest lines and trough lines are identified, six of which spanned through the whole domain. Five crest line bifurcations and 10 crest line terminations are recognized. A total of 3,640 bedforms measurements are made along the 400 analyzed transects. The bedforms have an average wavelength of 57 m and a height of 1.25 m (Table 3) with a best fit of $H_b = 0.01 L_b^{0.63}$ (Figure 6c). The bedforms are clearly asymmetrical, with a very gentle stoss side having an average angle of 1.9° and lee side having an average angle of 3.73°. The average lee side slope is therefore gentle and certainly very far from the angle of repose (30°). The average lee side angle of automatically detected bedforms, that is, as shown in Figure 6a, is 4.32°, showing the small influence of the manual positioning of crest and trough positions compared to automatic detection. Forty slip face portions are identified. In total, 84% of measured bedforms have a slip face, the remaining 16% have lee sides which slopes never exceed 15°. Slip face height is around 0.74 bedform height (Figure 6d), and no significant relation is found between slip face angle and lee side angle (Figure 6e). The histogram of lee side and slip face angles (Figure 6f) clearly shows how lee side angles are gentle and slip face angles are steep, being on average more than 23° (Table 3). The normalized slip face position is calculated as the position of the slip face beginning and end compared to the crest and trough positions and normalized by the lee side length. A normalized position of 0 is at the crest, and a normalized position of 1 is at the trough. As also visually recognized on Figure 6b, the slip faces are mainly situated close to the trough and away from the crest, having an average normalized beginning and end at 0.67 to 0.76 between crest and trough

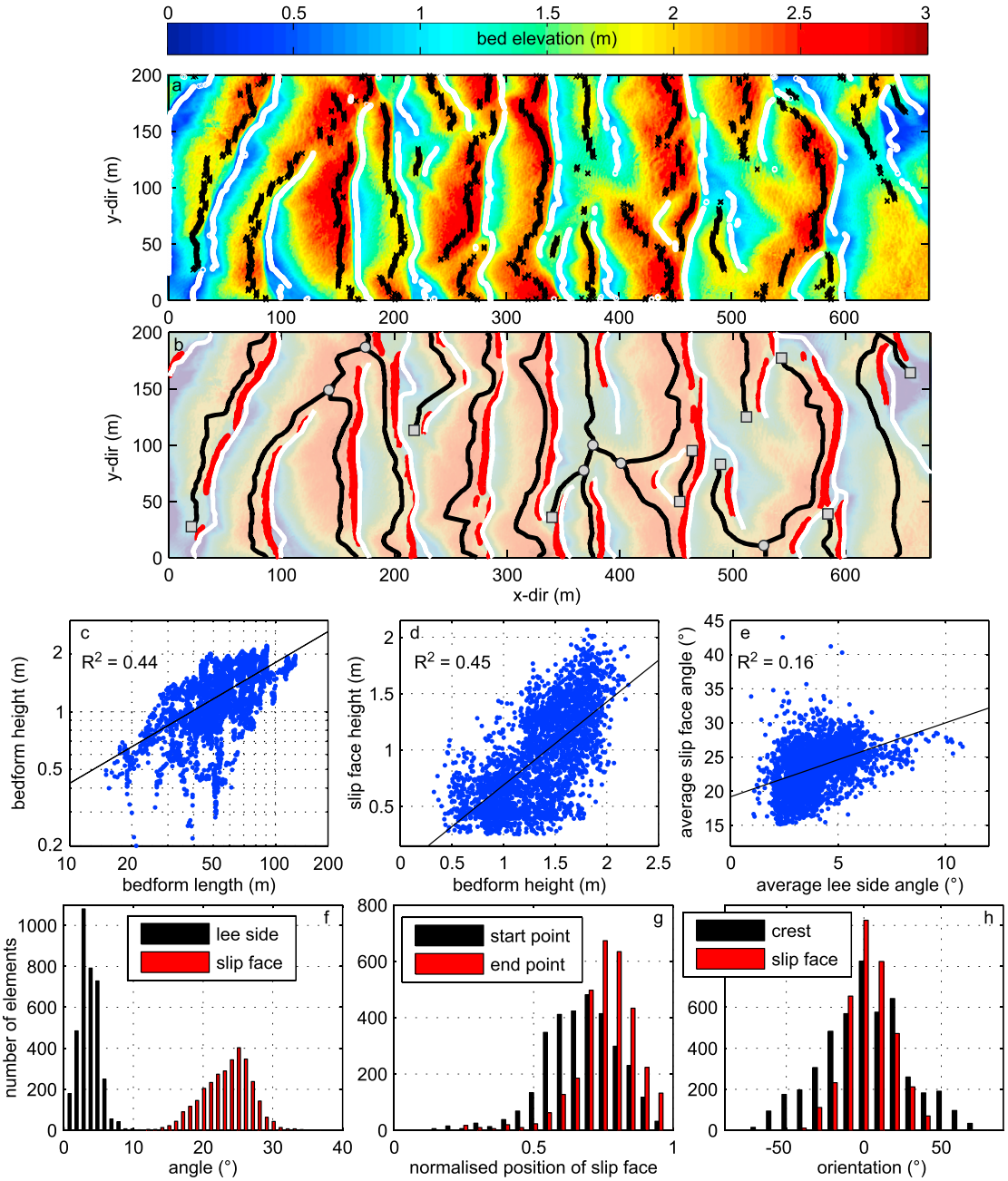

Figure 6. Bed height of the model domain with (a) crest (black crosses) and trough (white crosses) position determined with a zero-crossing technique applied on filtered bed height profiles and (b) crest lines (black), trough lines (white), contour of angles steeper than 15° (red), crest line terminations (gray squares), and crest line bifurcations (gray circles); (c) bedform length (L_b) versus bedform height (H_b), black line shows best fit $H_b = 0.01 L_b^{0.63}$ ($R^2 = 0.44$, number of elements n = 3,640); (d) slip face height H_{sf} versus bedform height, black line shows best fit $H_{sf} = 0.74\ H_b - 0.05$ ($R^2 = 0.45$, n = 3,053); (e) average slip face angle α_{sf} versus average lee side angle α_l, black line shows best fit $\alpha_{sf} = 1.08\ \alpha_l + 19.20$ ($R^2 = 0.18$, n = 3,053); (f) histogram of lee side and slip face angles; (g) histogram of the normalized position of the slip face start and end point; and (h) histogram of the crest and slip face orientation.

(Figure 6e and Table 3). This shows the presence of a well-developed crestal platform already identified by Parsons et al. (2005) and Gutierrez et al. (2013).

As described in Parsons et al. (2005), bedform crest line shapes vary from straight to lobe and saddle. The nondimensional span (NDS) measures the crest line curvature as the ratio of the length of the sinuous crest lines compared to a straight line (Venditti et al., 2005). Calculated for the 18 crest lines from the model domain, it varied between 1.1 and 1.4 with an average value of 1.2, which is the value proposed by

Table 3
Results of the Analysis of Bedform Morphology

Parameter	Average	Standard deviation	Minimum	Maximum
Number of bedforms	3,640			
Bedforms with a slip face	84%			
Bedform length (m)	57.27	19.29	15.00	125.00
Bedform height (m)	1.25	0.41	0.20	2.21
Stoss side mean angle (°)	1.95	0.57	0.04	3.94
Lee side mean angle (°)	3.73	1.45	0.20	10.78
Slip face mean angle (°)	23.37	3.49	9.93	42.52
Slip face normalized start position	0.67	0.13	0.16	0.97
Slip face normalized end position	0.76	0.11	0.23	1.00
Nondimensional span (NDS) crest	1.19	0.09	1.08	1.36
Nondimensional span (NDS) slip face	1.01	0.01	1.00	1.05

Venditti et al. (2005) as a threshold to differentiate between 2-D and 3-D bedforms. The crest lines are therefore not highly sinuous. However, the high number of bifurcation and termination indicates that the bedform field is still three-dimensional, through crest lines discontinuities if not through crest line curvature. The NDS is also calculated for each slip face portion. It is on average 1.01 with a maximum of 1.05 (Table 3) showing that the slip faces have very little curvature.

In order to further quantify the bedform three-dimensionality, the crest and slip face orientations compared to the flow are calculated: Each crest line or slip face portion is defined as a curve using a smoothing spline. The orientation of each point of the curve is then calculated as the angle of the curve compared to the y axis, an orientation being 0° if the crest or slip face is perfectly in line with the y axis (i.e., transverse to the flow), positive if the curve is bent toward the positive x or negative if the curve is toward the negative x. Both the crest lines and slip faces are on average transverse (average orientations of 0.6° and 3.2°, respectively). However, the crest lines show a much larger range of orientation that the slip faces (standard deviation of 27.3° and 14.8°, respectively; Figure 6h). This further highlights the more pronounced three-dimensionality of the crests compared to the two-dimensionality of the slip faces.

4.4. Flow and Turbulence

The main analysis of flow properties is shown for the simulation carried out with a bed roughness of 10^{-4} m and an input velocity of 1 m/s, which resulted in a domain-averaged velocity of 1.15 m/s. In this section, the results of the depth-averaged properties are first presented. The methodology used to further analyze the 3-D patterns of flow separation and turbulent wake is then detailed, before presenting their results. Finally, the influences of roughness length, grid size, and velocity on the results are examined.

4.4.1. Depth-Averaged Values

The water level (Figure 7a) shows pattern opposite to the bed elevation, with low water levels over the crests and high water levels over the troughs. The variations of water level are small, with a maximum amplitude of 4 cm created by bedform with an average height of 1.25 m in an average water depth of 6.42 m. The depth-averaged stream-wise velocity (Figure 7b) shows the expected patterns of flow acceleration over the stoss side and flow deceleration over the lee side. More precisely, fast flow is found over the upper stoss side, crest and beginning of the lee side, and flow slows down over the slip face, the parting point between fast and slow flows being the beginning of the slip face (the brink point) and not the crest. The depth-averaged cross-stream velocity (Figure 7c) is overall small, being on average only 2% of the stream-wise velocity. The topographic forcing of the flow is seen as a strong cross-stream velocity observed in regions where the crest or slip faces are curved (Figure 7c, Circle A) or where lateral height variations of the bed are encountered (Figure 7c, Circle B). The depth-averaged vertical velocity (Figure 7d) is also generally small, on average around 1% of the stream-wise velocity. It follows the expected patterns above bedforms, with upward velocity above the stoss sides and downward above the lee sides, with the strongest downward velocity found over the slip faces (average vertical velocity above the slip faces of −0.03 m/s, or 3% of average stream-wise velocity).

No turbulence is set at the entrance boundary. Therefore, the depth-averaged TKE (Figure 7e) is 0 m^2/s^2 at the beginning of the model domain and increases along the domain until approximately the sixth bedform

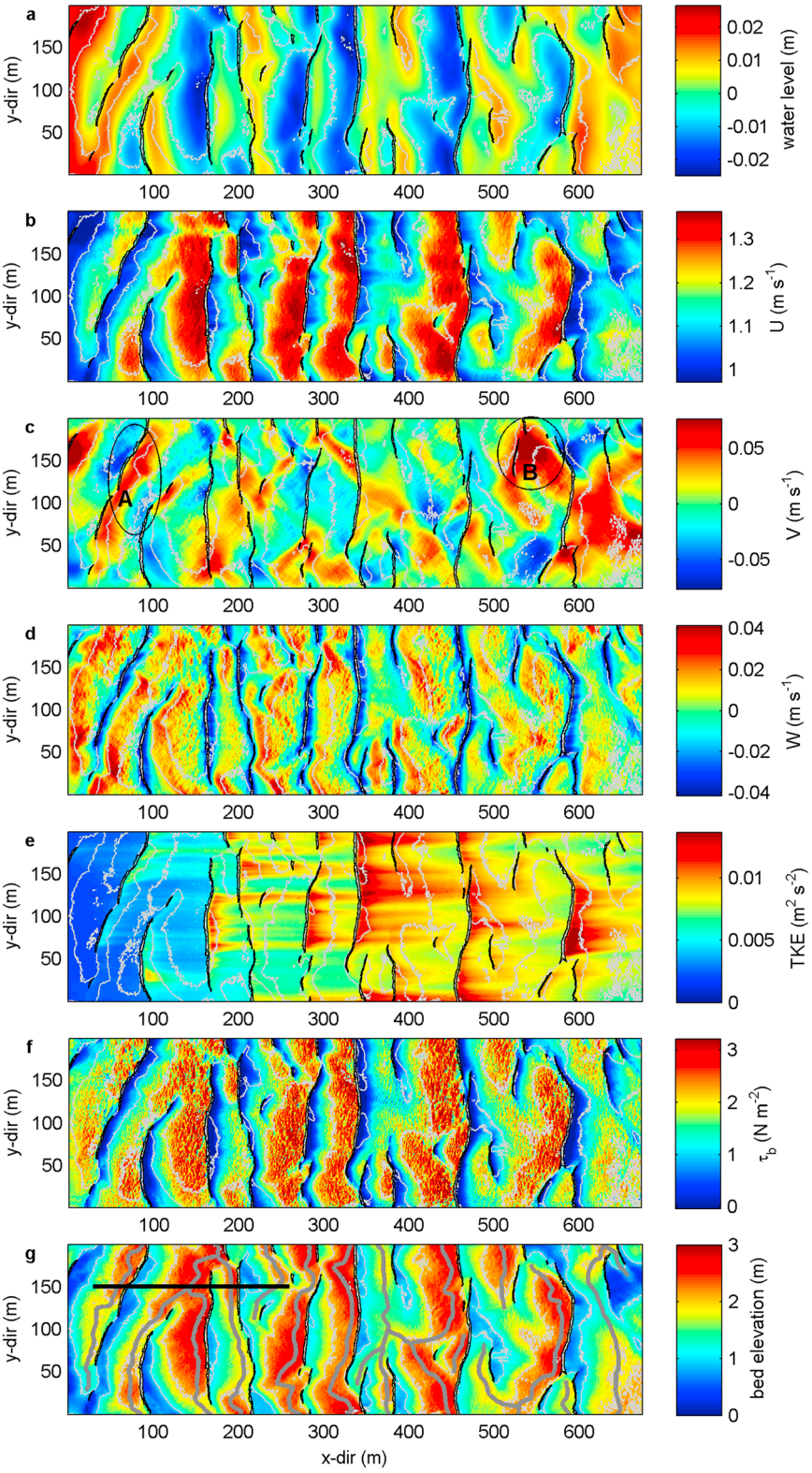

Figure 7. (a) Water level; (b) depth-averaged stream-wise velocity (U); (c) depth-averaged cross-stream velocity (V); (d) depth-averaged vertical velocity (W); (e) depth-averaged turbulent kinetic energy (TKE); (f) bed shear stress (τ_b); and (g) bed elevation in the model domain; in all figures, the black lines show the position of the slip faces, and the thin gray lines highlight the bed elevation contours; in (g), the thick black line indicates the profile shown in Figure 8, and the thick gray lines show the crest line positions; flow is from left to right.

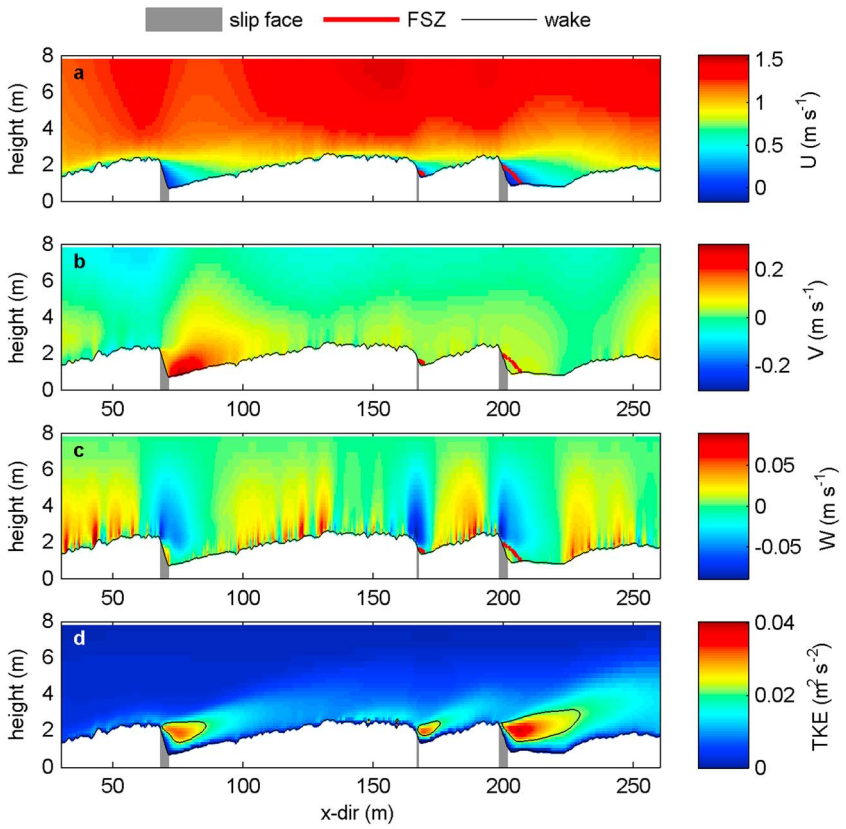

Figure 8. (a) Stream-wise velocity (U); (b), cross-stream velocity (V); (c) vertical velocity (W); and (d) turbulent kinetic energy (TKE) along a profile shown in Figure 8; flow is from left to right. FSZ = flow separation zone.

(at around $x = 350$ m), after which it is relatively stable from one bedform to the next. A strong increase in depth-averaged TKE is observed from the start of most slip faces, slowly fading to a background value in the stream-wise direction. This pattern shows the presence of a turbulent wake forming over the bedform slip face (see also Figure 8d). Over the lee of bedforms without a slip face, no increase of TKE is observed, indicating that a turbulent wake forms only if a portion of the lee face is steep enough, that is, a turbulent wake forms only if a slip face (lee side angle > 15°) is present.

The bed shear stress (Figure 7f) increases from troughs to crests, being slightly negative (i.e., shear stress applied toward the negative x direction) in areas of reverse flow. This pattern suggests high sediment mobilization and transport over the middle to high stoss side until the slip face where it is deposited and avalanches, keeping a steep slip face. Sediment may be trapped in the FSZ due to the reverse flow there. This agrees well with bed load models needed to numerically develop bedform (van Duin et al., 2017). In areas of bifurcation, the shear stress stays high, and no sediment is likely to deposit, showing that bifurcations are likely to be dominant transport paths as described by Allen (1968). Bifurcations may also be areas of dune pattern instability and enhanced deformation (Reesink et al., 2018).

4.4.2. Methodology to Analyze the 3-D Patterns

In order to better assess the mutual influence of bed morphology and flow properties, the 3-D positions of the FSZ and turbulent wake are calculated. The FSZs are defined as portions of the flow where negative stream-wise velocity are found. In order to remove isolated points coming from flow separation developing over large superimposed bedforms, only portions having at least four horizontally interconnected points (a FSZ of 4×0.5 m or 1 m^2) are kept for analysis (3.3% of the points are removed). The height of the FSZ is calculated for each point where a negative velocity is found as the height above the bed where the upstream directed flow is compensated by the downstream directed flow (Figure 1c). Along each transect and between successive crests, the length of the FSZ (L_{FSZ}) is calculated as the horizontal distance between the first and the last negative velocity point. The wake is detected as positions where TKE is higher than the TKE 98th percentile,

TKE_{98} (Figure 8d). In the case of the simulation with $z_0 = 10^{-4}$ m and input velocity of 1 m/s, $TKE_{98} = 0.026$ m^2/s^2. Again, in order to remove isolated points coming from the wake developing above large secondary bedforms, only portions having at least 36 horizontally or vertically interconnected points (36×0.5^2 or 9 m^3) are kept for analysis (0.7% of the points are removed). Along each transect and between each successive crests, the extent of the wake is calculated as the area occupied by TKE larger than TKE_{98}. The length of the wake (L_w) is calculated as the horizontal distance between the first point of the slip face and the maximum horizontal extent of the wake.

4.4.3. Results of Flow Separation and Turbulent Wake Analysis

Figure 9a shows the position of the detected FSZ and turbulent wake in relation to the bedform crest lines and slip faces. FSZs and turbulent wakes form over slip faces and are absent above bedforms with a gentle lee side. A FSZ is found behind 87.4% of the slip face measurements. Flow separates on average 0.95 m (or two grid cells) after the beginning of a slip face. The length of the FSZ is poorly related to the bedform height $L_{FSZ} = 3.45\ H_b + 0.16$ ($n = 2{,}637$, $R^2 = 0.13$, Figure 9b; hereafter n refers to the number of points and R^2 to the coefficient of determination). However, it is strongly related to the height of the slip face (H_{sf}) $L_{FSZ} = 5.05\ H_{sf}$ ($n = 2{,}811$, $R^2 = 0.74$; Figure 9c). Lefebvre et al. (2016) determined from a limited number of numerical model experiments that the relative length of the FSZ (length of flow separation normalized by the slip face height) is related to the slip face angle (α_{sf}): $L_{FSZ}/H_{sf} = 0.55\ \alpha_{sf} - 9.23$. Here no significant relation is found between relative length of the FSZ and slip face angle ($R^2 = 0.16$). However, including the average slip face angle to the height of the slip face helps in predicted the flow separation length: $L_{FSZ} = 0.23\ H_{sf}\ \alpha_{sf} - 0.72$ ($n = 2{,}811$, $R^2 = 0.82$; Figure 9d). Looking at the properties of the slip faces behind which there is a FSZ (87.4% of all measured slip faces), it appears that a flow separation is more likely to happen behind a slip face transverse to the flow compared to one which has an oblique orientation to the flow direction (Figure 9h). This can also be seen on Figure 8: Slip Faces 1 and 3 have similar properties apart from their orientation: length = 3.5 m, height = 1.6 and 1.4 m, average slopes = 24° and 21°, and orientation to the flow = 34.7° and −3.4°, respectively. Flow separates over Slip Face 3, which is transverse to the flow and not over Slip Face 1 due its oblique orientation to the flow. The suppression of flow reversal with slip face orientation to the flow is likely to be caused by the development of a strong cross-stream flow over an oblique slip face. For example, Figure 8b shows a strong positive cross-stream velocity over Slip Face 1 (oblique to the flow, orientation 34.7°), which is not present over Slip Face 3 (transverse to the flow, orientation −3.4°). A measure of this relation between slip face orientation and cross-stream flow intensity over the whole domain is illustrated in Figure 9j, which shows the relation between the average cross-stream velocity (averaged horizontally between the beginning of the slip face and a distance of 10 slip face height and vertically between the bed and the height of the slip face) and the slip face orientation.

The presence of a FSZ is also strongly related to the maximum angle of the slip face slope (Figure 9i). Lefebvre et al. (2016) and Kwoll et al. (2016) showed that over regular bedforms, the size of the flow separation increases with increasing slip face angle. In the present case, it is difficult to differentiate between the absence of flow separation and a shortening of the FSZ with decreasing maximum slip face angle. When a flow separation is less than four horizontal grid cells (4×0.5 m or 1 m^2), it is not detected. The observed relation between presence of reverse flow and maximum slip face angle seems to indicate that over natural bedforms, the maximum slip face angle influences the presence and/or size of flow separation. For a given average slip face angle, the flow is more likely to reverse or form a large FSZ when the maximum angle of the slip face is large than when it is gentle. The distribution of flow separation presence can be used to estimate the likelihood of finding a flow separation based on slip face properties. A FSZ is predicted to be present (absent) over a slip face with absolute orientation less (more) than 25° and a maximum angle steeper (less steep) than 20°. The presence or absence of a FSZ behind slip faces based on these properties is correctly predicted for 88.2% (3054) of all slip faces measurements (3,463). The threshold values of slip face orientation and maximum angle were found by adjusting the coefficients to find the best overall prediction of absence/presence.

A turbulent wake is found behind 80.6% of the slip face measurements. The length of the wake shows a weak relation to bedform height $L_w = 9.9\ H_b$ ($n = 2{,}309$, $R^2 = 0.08$; Figure 9e) but a strong relation to slip face height $L_w = 13.3\ H_{sp}$ ($n = 2{,}443$, $R^2 = 0.70$; Figure 9f). The extent of the wake is also strongly related to

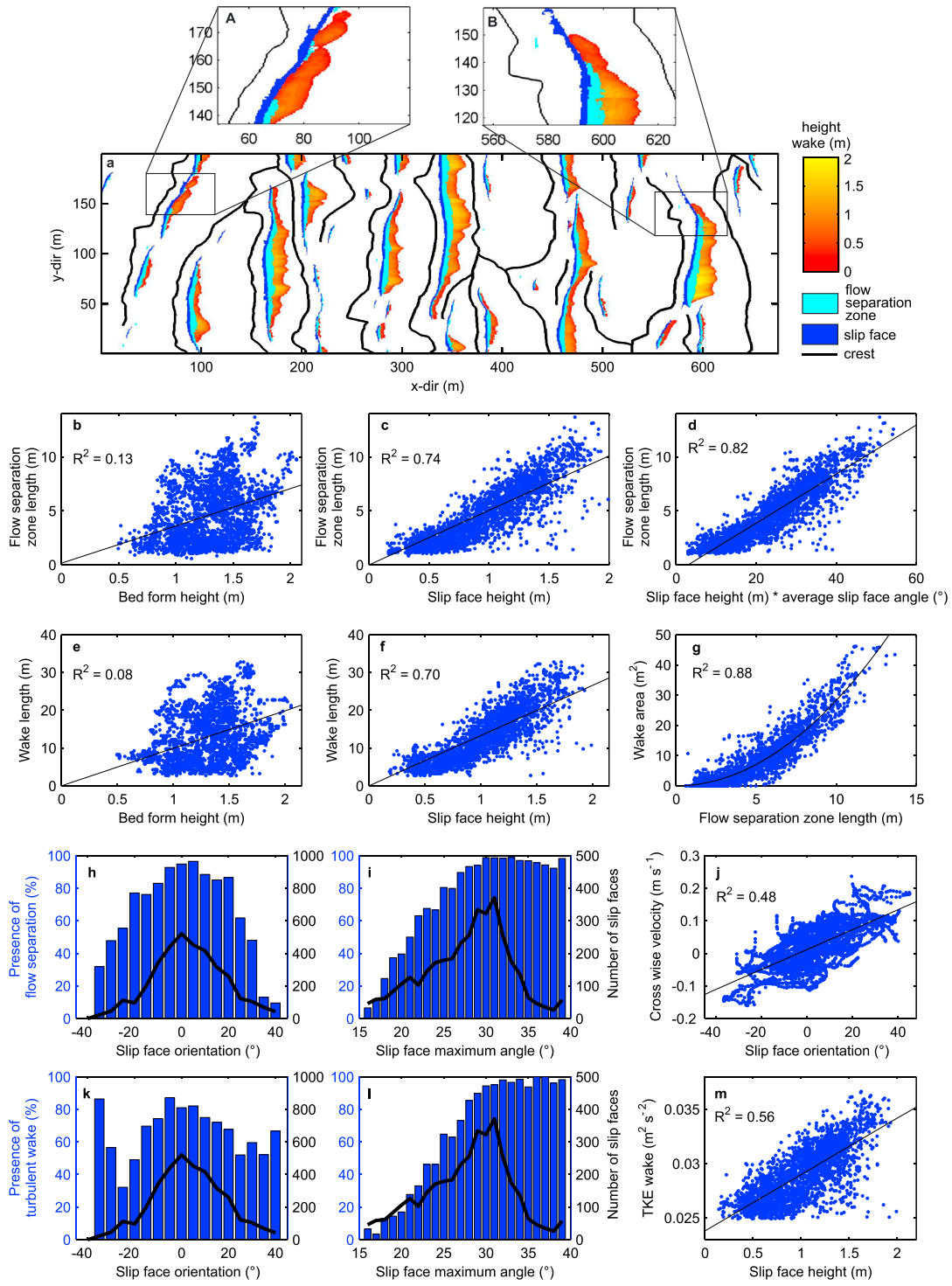

Figure 9. (a) Position of the crest lines, slip faces, and flow separation zone and height of the wake (vertical distance between the lowest and highest point of the wake) across the model domain, flow is from left to right; flow separation zone length as a function of (b) bedform height, (c) slip face height, and (d) slip face height * average slip face angle; length of the wake as a function of the bedform height (e) and slip face height (f) and extent of the wake as a function of the length of the flow separation zone (g); percentage of slip faces behind which there is flow separation as a function of (h) slip face direction and (i) slip face maximum angle; average cross-stream velocity behind slip faces as a function of slip face direction; percentage of slip faces behind which there is a turbulent wake as a function of (k) slip face direction and (l) slip face maximum angle; and (m) average turbulent kinetic energy (TKE) within the turbulent wake as a function of slip face height.

the length of the FSZ: extent of the wake = 0.28 L_{FSZ}^2 (n = 2,831, R^2 = 0.88; Figure 9g). Similarly to the FSZ, the wake is more likely to appear behind slip faces with a steep maximum angle than behind a slip face without a steep maximum angle (Figure 9l). However, the orientation of the slip face compared to the flow has a less prominent effect on the presence of a wake than on the presence of a FSZ (Figure 9k). This is partly due to turbulence advection over transverse slip faces, as can be seen in Figure 9a(A). There, a large flow separation and turbulent wake form over the slip face with transverse orientation to the flow and turbulence is advected by the strong cross-stream flow (see also Figure 7c, Highlight A) over the oblique part of the slip face. Although many oblique slip faces lack turbulent wake, in some places, the wake appears to simply form over an oblique slip face (Figure 9a(B)). Therefore, the presence of a wake is not too sensitive to slip face orientation. Similarly to flow separation, the distribution of wake presence is used to estimate the likelihood of finding a wake based on slip face properties. However, only the maximum slip face angle seems to be a determining criteria. A wake is predicted to be present (absent) over a slip face with a maximum angle steeper (less steep) than 25°. The presence or absence of a wake behind slip faces based on the maximum slip face angle is correctly predicted for 82.9% (3,022) of all measurements of slip faces (3,567).

4.4.4. Sensitivity to Input Parameters

The input velocity has little effect on the overall pattern of velocity and turbulence and mainly changes their absolute values, as recognized by Lefebvre, Paarlberg, and Winter (2014) over 2-D bedforms. Input roughness length has some influence on the results. The grid resolution of 0.5 m means that the superimposed bedforms are at the limit of the model resolution, as they are represented by one to five model cells, depending on their size. The highest roughness tested, $z_0 = 10^{-2}$ m, was meant to reproduce their roughness. Using this high bed roughness significantly alters the TKE patterns: In this case, the superimposed bedforms also create a large turbulent wake, which has the same strength as the wake from the primary bedforms. This pattern is unlikely to be true, the superimposed bedforms are therefore large enough to be resolved in the model and do not need to be parameterized. This simulation was not further considered. The difference between simulations with roughness lengths $z_0 = 2 \times 10^{-4}$ and 10^{-6} m is observed to be small. Lefebvre, Paarlberg, and Winter (2014) showed that high roughness length ($>10^{-3}$ m) has a strong influence on flow separation length whereas small roughness length (10^{-6} m $< z_0 < 10^{-3}$ m) has only little influence on flow separation length, which is confirmed by the present results. The simulation carried out with a roughness length $z_0 = 10^{-4}$ m is used as the reference case in section 4.4.3. However, a shortening of the FSZ length from 5.4 H_{SF} to 4.9 H_{SF} is recognized as roughness length increases from 10^{-6} m to 2×10^{-4} m. Again, this follows results from Lefebvre, Paarlberg, and Winter (2014) over 2-D angle-of-repose bedforms, who observed a shortening of the flow separation length with increasing roughness. However, the change in flow separation length is small compared to the roughness length variations, and a value of 5 H_{SF} is a good estimate of FSZ length. The chosen roughness length at field scale is also close to that determined as fitting best the roughness used for the model verification against laboratory measurements of Maddux et al. (2003). This may be because during the laboratory experiments, the dunes were covered with sand to reproduce a realistic roughness.

Simulations carried out with a coarser grid of 1 m showed similar patterns and trends to those run with a fine grid of 0.5 m. However, a smoothing or flattening of the bed is recognized when the resolution is decreased. Therefore, the angles are gentler for the 1-m grid than for the 0.5-m grid. As a result, the relations between the flow and bed properties changed. For example, with a resolution of 1 m, the length of the FSZ and the length of the wake are related to the height of the slip face through L_{FSZ} = 4.62 H_{sf} (n = 978, R^2 = 0.57) and L_w = 13.6 H_{sf} (n = 979, R^2 = 0.61).

5. Discussion

One of the key findings of this work is that the presence and size of the FSZ and turbulent wake relate to the presence and properties of the slip face (specifically maximum angle and orientation to the flow) more than to that of the crest line or bedform height. This is in agreement with the results of Lefebvre et al. (2016) and with the implicit statements of other authors (e.g., Kostaschuk, 2000; Lefebvre, Paarlberg, & Winter, 2014) who determined the presence of reverse flow based on the angle of the steepest portion of the lee side, that is, the slip face. The slip face has been described here as the part of the lee side with an angle of 15° or steeper. Taking a threshold angle of 13° to 17° gave similar results (e.g., L_{FSZ} = 5.16 H_{sf}, n = 2,998, R^2 = 0.74 and L_{FSZ} = 5.77 H_{sf}, n = 2,959, R^2 = 0.75 for the threshold to define slip face put at 13° and 17°, respectively). The value

of 15° is kept as it is intermediate between the "10° and 20°" commonly cited as a threshold for the formation of reverse flow (Best & Kostaschuk, 2002; Kostaschuk & Villard, 1996; Paarlberg et al., 2007) and the 11–18° determined by Lefebvre et al. (2016) from numerical simulations. We therefore advocate that bedform fields should be characterized not only by the positions of the crest and trough lines but also the slip face presence and position in order to correctly predict the presence and size of reverse flow and turbulent wake. We propose simple relations ($L_{FSZ} = 5\ H_{SF}$ and $L_W = 13\ H_{SF}$) to calculate these values based on a bathymetric map. These relations are valid for slip faces with a maximum angle of 20° or steeper and with an orientation to the flow of 25° or less. It should be noted that these values were determined from a model validated only from laboratory measurements and uncalibrated at field scale. Therefore, the relations are given only as estimates. These estimates fit well with previous field, laboratory, and numerical results, which usually give the length of the flow separation as 4 to 6 times the bedform height (in case of a simple lee side) or slip face height (Engel, 1981; Lefebvre, Paarlberg, & Winter, 2014; Paarlberg et al., 2007). The relation between turbulent wake length and slip face or bedform height has rarely been estimated. The definition of turbulent wake itself is still unclear. In this study, it was taken as where the TKE was greater than TKE_{98}. Kwoll (2013) defined the vertical extent of the wake as the height above the bed at which the vertical profile of the TKE adopts a linear form toward the water surface. This gave a very large wake, which extends along the whole bedform and relatively high in the water column (see, e.g., her Figure 4.7). Lefebvre, Paarlberg, Ernstsen, et al. (2014) defined the wake as the region where TKE is at least 70% of the maximum TKE above individual bedforms. Keeping with the definition proposed here, the turbulent wake calculated from the laboratory measurements of Maddux et al. (2003) is around 6 times the bedform height (in this case equal to the slip face height). However, taking the threshold of Lefebvre, Paarlberg, Ernstsen, et al. (2014) of TKE_{70}, the turbulent wake is 10 to 17 H_b. A consistent and meaningful definition of the turbulent wake still needs to be established.

Bedform height is only poorly related to slip face height (Figure 6d), and slip face orientation compared to the flow is found to vary less than the crest line orientation (Figure 6h). Therefore, assessing the presence of reverse flow based on bedform height and crest line orientation may produce misleading results. However, more data from varied environments are needed to test the universality of the proposed relations. Of course, such an analysis also requires to be mindful of the original resolution of the available data. Simulation results show that the resolution of the grid has an impact on the results because a coarser resolution flattens the angles. Therefore, caution should be taken to use these relations to bathymetric data with a much coarser (e.g., 5 m) resolution.

Over the natural bedform studied here, the size of the FSZ and the turbulent wake is related to the slip face height more than to the bedform height. It has important consequences in the calculation of bedform roughness. Bedform roughness is commonly calculated using bedform height as a main input, together with bedform length and water depth, depending on the formula (e.g., Bartholdy et al., 2010; Engelund, 1977; Soulsby, 1997; Vanoni & Hwang, 1967). Following the initial work of Ogink (1989) and Van Rijn (1993), Lefebvre and Winter (2016) introduced the use of the lee side angle to calculate bedform roughness in order to take into account the fact that bedforms with a gentle lee side produce little turbulence and roughness compared to bedforms with a steep lee side, which produce strong turbulence and roughness. Bedform roughness formulas have traditionally used bedform height as a parameter because they were based on experiments conducted with triangular bedform, where the lee side is made of one segment. Natural bedforms in the field are likely to possess a brink point, with a lee side made up of two or more segments (Lefebvre et al., 2016) Therefore, formulas used to calculate the roughness of natural bedform with a complex morphology may have to be adapted to use slip face height and angle instead of bedform height and lee side angle in order to more accurately calculate the roughness of natural bedform.

Venditti (2007) observed that flow recirculation and turbulence were enhanced over lobe-shaped dune crest lines and reduced over saddles compared to over 2-D dunes. Parsons et al. (2005) on the other hand measured smaller FSZs over both lobe- and saddle-shaped bedforms than over 2-D bedforms. A relation between flow separation size and crest line properties could not be observed in the present work. Instead, flow separation is found to be controlled by slip face orientation. However, slip faces in the study area are relatively straight (average NDS 1.01), without lobes and saddles. The influence of slip face orientation, if not sinuosity, is seen as a suppression of flow separation when the slip face has an orientation of 25° or more compared to

Table 4
Effect of Lee Slope Shape and Three-Dimensionality on Flow Separation and Turbulent Wake

Property	Gentle slope	Threshold	Steep slope
Steepness of the slope	No permanent flow separation (Best & Kostaschuk, 2002; Kostaschuk & Villard, 1996) Weak and vaguely defined wake (Kwoll et al., 2016; Lefebvre et al., 2016)	Lee side angle of 10–20° (Best & Kostaschuk, 2002; Kostaschuk & Villard, 1996; Kwoll et al., 2016; Paarlberg et al., 2007) Maximum lee side angle over a horizontal distance of 5 m of 10° Lee side angle of 11–18° (Lefebvre & Winter, 2016) Slip face angle 15° (this study)	Permanent flow separation and strong wake (see review by Best, 2005)
	Simple steep lee side	Compound slope (crestal platform and steep slip face)	
2-D	Flow separation zone starting at the crest and extending four to six bedform height (Engel, 1981; Paarlberg et al., 2007; Lefebvre, Paarlberg, & Winter, 2014) Strong wake starting at the crest and extending downstream, size influenced by roughness length, relative height, and aspect ratio (Lefebvre, Paarlberg, & Winter, 2014)	Flow separation starting at brink point and extending four to six slip face height (Paarlberg et al., 2007; Lefebvre et al., 2016, this study) Turbulent wake size starting at brink point, length related to flow separation length (Lefebvre, Paarlberg, Ernstsen, et al., 2014, this study), wake length around 13 slip face height (this study)	
3-D	Over the node or a saddle shape, reduced flow separation zone, and suppressed wake. Over the centerline or lobe shape, strong flow separation, and upward diffused wake (Maddux et al., 2003; Venditti, 2007; Omidyeganeh & Piomelli, 2013) Importance of upstream bed configuration (Venditti, 2007)	No flow separation zone for slip faces with an orientation of around 25° or more compared to the mean flow (this study) Turbulent wake affected by slip face orientation but can also be advected over the slip face (this study)	

the flow due to the strengthening of the cross-stream flow. However, in the study area, only 11% of the slip faces have an orientation more than 25° to the flow. These findings highlight that the relative contributions of slip face sinuosity and orientation to flow separation require further quantification over bedforms having sinuous slip faces (with pronounced lobe and saddle shapes) and/or having an oblique orientation to the flow (with many slip faces having an orientation >25° to the flow). This is especially important because flow separation controls the dynamics of deposition (Allen, 1982; Reesink & Bridge, 2009) and bed roughness (Kostaschuk & Villard, 1996; Lefebvre & Winter, 2016; Smith & McLean, 1977)

Results from Venditti (2007) and Maddux et al. (2003) also suggest that turbulence properties are affected by crest lines sinuosity and height variations, with an upward suppression of turbulence in regions where a strong cross-stream flow develops (Figure 1). In the present work, no systematic relation is found between turbulent wake height, length, or extent and slip face orientation or strength of the cross-stream flow. The results from Venditti (2007) and Maddux et al. (2003) may be due to the regularity of the investigated bedforms. Bedform regularity may have enhanced flow patterns which do not develop over natural bedform showing a strong variability in shape. For example, Venditti (2007) observed no flow separation and turbulent wake over irregularly placed bedforms and emphasized the importance of upstream bed configuration. Over a natural bedform field, the variations of upstream and cross-stream morphology create complicated flow pattern, interacting with each other in ways which are not recognized over regular bedforms, and vertical suppression or diffusion of turbulence due to slip face orientation may not take place.

The influence of lee side slope shape and three-dimensionality are summarized in Table 4. The present study contributes in a better characterization of the influence of compound slope on flow separation and turbulent wake. Some important aspects of interaction between flow and natural 3-D bedforms investigated in the present study are illustrated in Figure 10. The plan view (Figure 10a) exemplifies the absence of reverse flow and the suppression of turbulence associated with the cross-stream which develops over slip faces which have an orientation of 25° or more to the main flow direction. The turbulent wake may also be advected over such

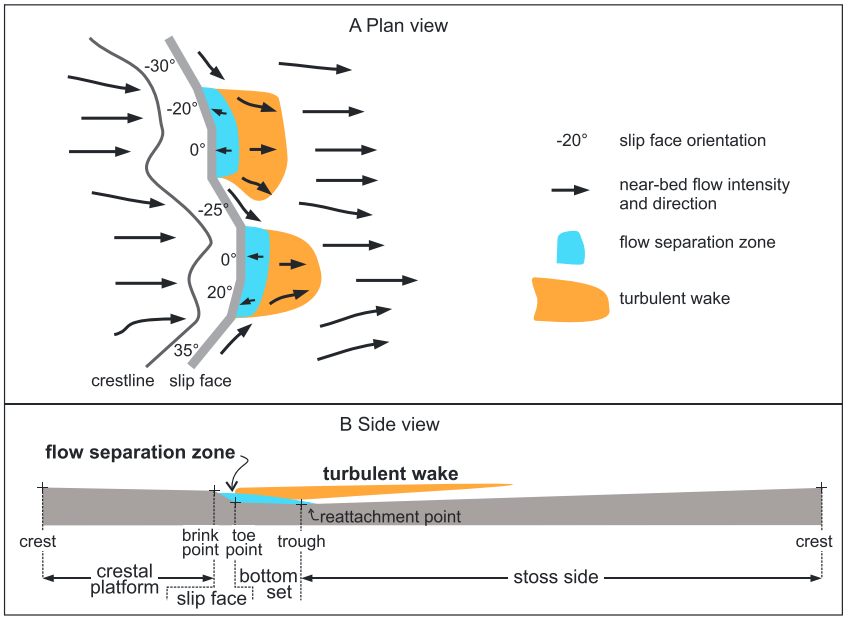

Figure 10. Summary of some flow properties over 3-D bedform as observed at the study site; (a) plan view showing the influence of 3-D morphology, with an absence of flow separation over slip faces oriented more than 25° to the main flow direction; (b) side view illustrating the typical size of flow separation and turbulent wake as a function of slip face height (no vertical exaggeration, dimensions represented as the average dimensions from the bedform field); morphological element nomenclature after Allen (1968).

oblique slip faces. Presence and size of flow separation and turbulent wake are controlled by slip face orientation and height and not by crest line properties. Figure 10b shows a bedform profile made from the average dimensions determined from the bedform field and flow property results from the model, without vertical exaggeration. The slip face, although small compared to the whole bedform, governs the size of the FSZ and the turbulent wake. It is interesting to note that the reattachment point is situated on average 0.66 m after the trough. The small distance between the end of flow separation and trough position suggests that the trough position is controlled by the flow separation size. It is likely that flow mobilizes sediment over the upper stoss side where bed shear stress is high. The sediment is transported over the crest and being deposited over the slip face, where it avalanches. Transport in the bottom set is controlled by the flow separation properties, with sediment already in motion being moved towards the toe point, thereby maintaining the trough as the lowest point as little sediment is deposited there (Herbert & Alexander, 2018).

6. Conclusions

A three-dimensional numerical model was set up using the Delft3D modeling system to simulate Reynolds-averaged flow properties, water level, and bed shear stress over bedforms. The model showed to correctly simulate flow velocity and turbulence when verified against laboratory data over idealized regular 3-D bedforms.

The model was used over a bedform field of the Río Paraná to bring insights in the relation between complex 3-D bed morphology and flow properties. The main conclusions of this work are the following:

1. The presence and size of the FSZ and turbulent wake depend on the presence, height, and maximum angle of the slip face (lee side angles >15°) and not necessarily on bedform height and the average lee side angle.
2. With the tested setting, the flow separation length can be estimated as being 5 times the height of the slip face. The length of the wake is around 13 times the slip face height.
3. The size of a FSZ is further controlled by the orientation and steepness of the slip face. If the slip face has an orientation of around 25° or more compared to the mean flow, a strong cross-stream flow develops,

and no reverse stream-wise flow forms. A reverse flow is more likely to be found over slip faces with a maximum angle of 20° or more.

4. The influence of slip face orientation to the flow was less pronounced for the presence of a turbulent wake than for the initiation of flow separation, because turbulent wake may also be advected over the slip face.

A detailed description of the bedform morphology including the presence and properties (height, maximum angle, and orientation) of the slip face is therefore necessary to correctly represent the complex interaction of flow and bedform. This has crucial implications for calculating bedform roughness and predicting flow and sediment dynamics over bedforms.

Acknowledgments
This study was funded by the German Research Foundation (Deutsche Forschungsgemeinschaft, DFG), Project 345915838. Results are available through the Publishing Network for Geoscientific & Environmental Data (PANGAEA, https://doi.pangaea.de/10.1594/PANGAEA.904402, http://www.pangaea.de). The author is very grateful to Tim Maddux and Dan Parsons for sharing their data. Many thanks to Christian Winter for fruitful discussion and helpful feedback and to Elda Miramontes for proofreading the near-final version of the manuscript. The insightful comments of an anonymous reviewer, Arjan Reesink, Jord Warmink, and the associate editor greatly helped in improving the manuscript.

References

Allen, J. R. L. (1968). *Current ripples*. New York, NY: Elsevier.

Allen, J. R. L. (1982). *Sedimentary structures: Their character and physical basis*. New York: Elsevier.

Baas, J. H. (1994). A flume study on the development and equilibrium morphology of current ripples in very fine sand. *Sedimentology*, *41*(2), 185–209. https://doi.org/10.1111/j.1365-3091.1994.tb01400.x

Baas, J. H., Best, J. L., & Peakall, J. (2016). Predicting bedforms and primary current stratification in cohesive mixtures of mud and sand. *Journal of the Geological Society*, *173*(1), 12–45. https://doi.org/10.1144/jgs2015-024

Bartholdy, J., Flemming, B. W., Ernstsen, V., Winter, C., & Bartholomä, A. (2010). Hydraulic roughness over simple subaqueous dunes. *Geo-Marine Letters*, *30*, 63–76. https://doi.org/10.1007/s00367-009-0153-7

Best, J. (2005). The fluid dynamics of river dunes: A review and some future research directions. *Journal of Geophysical Research*, *110*, F04S02. https://doi.org/10.1029/2004JF000218

Best, J., & Kostaschuk, R. (2002). An experimental study of turbulent flow over a low-angle dune. *Journal of Geophysical Research*, *107*(C9), 3135. https://doi.org/10.1029/2000JC000294

Casulli, V. (1999). A semi-implicit finite difference method for non-hydrostatic, free surface flows. *International Journal Numerical Methods In Fluids*, *30*(4), 425–440. https://doi.org/10.1002/(SICI)1097-0363(19990630)30:4<425::AID-FLD847>3.0.CO;2-D

Deltares (2014). *User manual Delft3D-FLOW*. Delft, The Netherlands: Deltares.

El Kheiashy, K., McCorquodale, J., Georgiou, I., & Meselhe, E. (2010). Three dimensional hydrodynamic modeling over bedforms in open channels. *International Journal of Sediment Research*, *25*(4), 431–440. https://doi.org/10.1016/S1001-6279(11)60010-3

Engel, P. (1981). Length of flow separation over dunes. *Journal of the Hydraulics Division*, *107*(10), 1133–1143.

Engelund, F. (1977). Hydraulic resistance for flow over dunes. Retrieved from

Ernstsen, V. B., Noormets, R., Winter, C., Hebbeln, D., Bartholomae, A., Flemming, B. W., & Bartholdy, J. (2005). Development of subaqueous barchanoid-shaped dunes due to lateral grain size variability in a tidal inlet channel of the Danish Wadden Sea. *Journal of Geophysical Research*, *110*, F04S08. https://doi.org/10.1029/2004JF000180

Fraccascia, S., Winter, C., Ernstsen, V. B., & Hebbeln, D. (2016). Residual currents and bedform migration in a natural tidal inlet (Knudedyb, Danish Wadden Sea). *Geomorphology*, *271*, 74–83. https://doi.org/10.1016/j.geomorph.2016.07.017

Gutierrez, R. R., Abad, J. D., Parsons, D. R., & Best, J. L. (2013). Discrimination of bedform scales using robust spline filters and wavelet transforms: Methods and application to synthetic signals and bedforms of the Río Paraná, Argentina. *Journal of Geophysical Research: Earth Surface*, *118*, 1400–1418. https://doi.org/10.1002/jgrf.20102

Gutierrez, R. R., Mallma, J. A., Núñez-González, F., Link, O., & Abad, J. D. (2018). Bedforms-ATM, an open source software to analyze the scale-based hierarchies and dimensionality of natural bedforms. *SoftwareX*, *7*, 184–189. https://doi.org/10.1016/j.softx.2018.06.001

Hardy, R. J., Parsons, D. R., Best, J. L., Lane, S. N., Kostaschuk, R., & Orfeo, O. (2006, 6-8 September 2006). Three-dimensional numerical modelling of flows over a natural dune field. Paper presented at the River Flow 2006: International Conference on Fluvial Hydraulics, Lisbon, Portugal.

Herbert, C. M., & Alexander, J. (2018). Bottomset architecture formed in the troughs of dunes and unit bars. *Journal of Sedimentary Research*, *88*, 522–553. https://doi.org/10.2110/jsr.2018.28

Khosronejad, A., Kozarek, J. L., Palmsten, M. L., & Sotiropoulos, F. (2015). Numerical simulation of large dunes in meandering streams and rivers with in-stream rock structures. *Advances in Water Resources*, *81*, 45–61. https://doi.org/https://doi.org/10.1016/j.advwatres.2014.09.007

Khosronejad, A., & Sotiropoulos, F. (2014). Numerical simulation of sand waves in a turbulent open channel flow. *Journal of Fluid Mechanics*, *753*, 150–216. https://doi.org/10.1017/jfm.2014.335

Khosronejad, A., & Sotiropoulos, F. (2017). On the genesis and evolution of barchan dunes: Morphodynamics. *Journal of Fluid Mechanics*, *815*, 117–148. https://doi.org/10.1017/jfm.2016.880

Kostaschuk, R. (2000). A field study of turbulence and sediment dynamics over subaqueous dunes with flow separation. *Sedimentology*, *47*(3), 519–531. https://doi.org/10.1046/j.1365-3091.2000.00303.x

Kostaschuk, R., Shugar, D., Best, J., Parsons, D., Lane, S., Hardy, R., & Orfeo, O. (2009). Suspended sediment transport and deposition over a dune: Río Paraná, Argentina. *Earth Surface Processes and Landforms*, *34*(12), 1605–1611. https://doi.org/10.1002/esp.1847

Kostaschuk, R., & Villard, P. (1996). Flow and sediment transport over large subaqueous dunes: Fraser River, Canada. *Sedimentology*, *43*(5), 849–863. https://doi.org/10.1111/j.1365-3091.1996.tb01506.x

Kwoll, E. (2013). Bedforms, macroturbulence, and sediment transport at the fluid-bed interface. (PhD Thesis), University of Bremen. Retrieved from https://elib.suub.uni-bremen.de/edocs/00103491-1.pdf

Kwoll, E., Venditti, J. G., Bradley, R. W., & Winter, C. (2016). Flow structure and resistance over subaquaeous high- and low-angle dunes. *Journal of Geophysical Research: Earth Surface*, *121*, 545–564. https://doi.org/10.1002/2015JF003637

Lefebvre, A., Paarlberg, A. J., Ernstsen, V. B., & Winter, C. (2014). Flow separation and roughness lengths over large bedforms in a tidal environment: A numerical investigation. *Continental Shelf Research*, *91*, 57–69. https://doi.org/10.1016/j.csr.2014.09.001

Lefebvre, A., Paarlberg, A. J., & Winter, C. (2014). Flow separation and shear stress over angle of repose bedforms: A numerical investigation. *Water Resources Research*, *50*, 986–1005. https://doi.org/10.1002/2013WR014587

Lefebvre, A., Paarlberg, A. J., & Winter, C. (2016). Characterising natural bedform morphology and its influence on flow. *Geo-Marine Letters*, *36*(5), 379–393. https://doi.org/10.1007/s00367-016-0455-5

Lefebvre, A., & Winter, C. (2016). Predicting bedform roughness: The influence of lee side angle. *Geo-Marine Letters*, *36*(2), 121–133. https://doi.org/10.1007/s00367-016-0436-8

Maddux, T. B., Nelson, J. M., & McLean, S. R. (2003). Turbulent flow over three-dimensional dunes: 1. Free surface and flow response. *Journal of Geophysical Research*, *108*(F1), 6009. https://doi.org/10.1029/2003JF000017

Malarkey, J., Baas, J. H., Hope, J. A., Aspden, R. J., Parsons, D. R., Peakall, J., et al. (2015). The pervasive role of biological cohesion in bedform development. *Nature Communications*, *6*, 6257. https://doi.org/10.1038/ncomms7257

McLean, S. R., Wolfe, S. R., & Nelson, J. M. (1999). Spatially averaged flow over a wavy boundary revisited. *Journal of Geophysical Research*, *104*(C7), 15,743–15,753. https://doi.org/10.1029/1999JC900116

Naqshband, S., Ribberink, J., & Hulscher, S. (2014). Using both free surface effect and sediment transport mode parameters in defining the morphology of river dunes and their evolution to upper stage plane beds. *Journal of Hydraulic Engineering*, *140*, 06014010. https://doi.org/10.1061/(ASCE)HY.1943-7900.0000873

Ogink, H. (1989). Hydraulic roughness of single and compound bedforms, part XI report on model investigations. Retrieved from

Omidyeganeh, M., & Piomelli, U. (2013). Large-eddy simulation of three-dimensional dunes in a steady, unidirectional flow. Part 1. Turbulence statistics. *Journal of Fluid Mechanics*, *721*, 454–483. https://doi.org/10.1017/jfm.2013.36

Paarlberg, A. J., Dohmen-Janssen, C. M., Hulscher, S. J. M. H., & Termes, P. (2007). A parameterization of flow separation over subaqueous dunes. *Water Resources Research*, *43*, W12417. https://doi.org/10.1029/2006WR005425

Parsons, D. R., Best, J. L., Orfeo, O., Hardy, R. J., Kostaschuk, R., & Lane, S. N. (2005). Morphology and flow fields of three-dimensional dunes, Rio Paraná, Argentina: Results from simultaneous multibeam echo sounding and acoustic Doppler current profiling. *Journal of Geophysical Research*, *110*, F04S03. https://doi.org/doi:10.1029/2004JF000231

Platzek, F. W., Stelling, G. S., Jankowski, J. A., & Pietrzak, J. D. (2014). Accurate vertical profiles of turbulent flow in z-layer models. *Water Resources Research*, *50*, 2191–2211. https://doi.org/10.1002/2013WR014411

Reesink, A. J. H., & Bridge, J. S. (2009). Influence of bedform superimposition and flow unsteadiness on the formation of cross strata in dunes and unit bars—Part 2, further experiments. *Sedimentary Geology*, *222*(3-4), 274–300. https://doi.org/10.1016/j.sedgeo.2009.09.014

Reesink, A. J. H., Parsons, D. R., Ashworth, P. J., Best, J. L., Hardy, R., Murphy, B. J., et al. (2018). The adaptation of dunes to changes in river flow. *Earth-Science Reviews*, *185*, 1065–1087. https://doi.org/10.1016/j.earscirev.2018.09.002

Rubin, D. M. (2012). A unifying model for planform straightness of ripples and dunes in air and water. *Earth-Science Reviews*, *113*, 176–185. https://doi.org/10.1016/j.earscirev.2012.03.010

Smith, J. D., & McLean, S. R. (1977). Spatially averaged flow over a wavy surface. *Journal of Geophysical Research*, *82*(12), 1735–1746. https://doi.org/10.1029/JC082i012p01735

Sotiropoulos, F., & Khosronejad, A. (2016). Sand waves in environmental flows: Insights gained by coupling large-eddy simulation with morphodynamics. *Physics of Fluids*, *28*, 021301. https://doi.org/10.1063/1.4939987

Soulsby, R. L. (1997). *Dynamics of marine sands: A manual for practical applications*. London: Thomas Telford.

Southard, J. B., & Boguchwal, L. A. (1990). Bed configuration in steady unidirectional water flows; part 2, synthesis of flume data. *Journal of Sedimentary Research*, *60*(5), 658–679. https://doi.org/10.1306/212F9241-2B24-11D7-8648000102C1865D

Stoesser, T. (2014). Large-eddy simulation in hydraulics: Quo vadis? *Journal of Hydraulic Research*, *52*(4), 441–452. https://doi.org/10.1080/00221686.2014.944227

Stoesser, T., Braun, C., García-Villalba, M., & Rodi, W. (2008). Turbulence structures in flow over two-dimensional dunes. *Journal of Hydraulic Engineering*, *134*(1), 42–55. https://doi.org/10.1061/(ASCE)0733-9429(2008)134:1(42)

Van der Mark, C. F., & Blom, A. (2007). A new and widely applicable tool for determining the geometric properties of bedforms. Retrieved from https://doi.org/10.13140/RG.2.2.17637.40161

Van der Mark, C. F., Blom, A., & Hulsher, S. J. M. H. (2008). Quantification of variability in bedform geometry. *Journal of Geophysical Research*, *113*, F03020. https://doi.org/10.1029/2007JF000940

van Duin, O. J. M., Hulscher, S. J. M. H., Ribberink, J. S., & Dohmen-Janssen, C. M. (2017). Modeling of spatial lag in bed-load transport processes and its effect on dune morphology. *Journal of Hydraulic Engineering*, *143*(2), 04016084. https://doi.org/10.1061/(ASCE)HY.1943-7900.0001254

Van Rijn, L. C. (1993). *Principles of sediment transport in rivers, estuaries and coastal seas*. Amsterdam: Aqua Publications.

Vanoni, V. A., & Hwang, L. S. (1967). Relation between bedforms and friction in stream. *Journal of the Hydraulics Division*, *93*(HY3), 121–144.

Venditti, J. G. (2007). Turbulent flow and drag over fixed two- and three-dimensional dunes. *Journal of Geophysical Research*, *112*(F4), F04008. https://doi.org/10.1029/2006JF000650

Venditti, J. G. (2013). Bedforms in sand-bedded rivers. In J. Shroder & E. Wohl (Eds.), *Treatise on geomorphology* (pp. 137–162). San Diego, CA: Academic Press. https://doi.org/10.1016/B978-0-12-374739-6.00235-9

Venditti, J. G., Church, M., & Bennett, S. J. (2005). On the transition between 2D and 3D dunes. *Sedimentology*, *52*(6), 1343–1359. https://doi.org/10.1111/j.1365-3091.2005.00748.x